JMEPEG
https://doi.org/10.1007/s11665-023-09000-2

1059-9495/$19.00

ORIGINAL RESEARCH ARTICLE

Experimental Analysis and Surface Morphology of Holes Made by Electrical Discharge Machining on $MoSi_2$-SiC Composite

L. Selvarajan, R. Rajavel, C. Arun, and C. Raju

Submitted: 10 January 2023 / Revised: 14 September 2023 / Accepted: 23 September 2023

A feasibility study of machining molybdenum disilicide–silicon carbide composites using copper electrodes was investigated and evaluated in this research. High-temperature tools, including extruders, metal shapers, turbine blades, ladles, and crucibles, have been fabricated from such composites. Molybdenum disilicide–silicon carbide composites are challenging to machine in conventional ways. With spark electrical discharge machining, manufacturers can easily satisfy geometric tolerances and accomplish accurate measurements. Measurement characteristics such as material removal rate (0.03124 g/min), top radial overcut (0.1395 mm), wear ratio (3.5812), surface roughness (0.295 μm), tool wear rate (0.00181 g/min), cylindricity (0.142 mm), bottom radial overcut (0.0898 mm), taper angle (5.8952), run out (0.145 mm), perpendicularity (0.019 mm), and circularity (0.172 mm) were evaluated by gray relational analysis during the sparking process. The most important machining factors were found to be current (34.6749%), sparking ON time (25.6502%), and gap voltage (12.0462%), and they were identified using an analysis of variance based on gray relational analysis. As the 23rd possible combination of experiment parameters, the best combination of results was determined as $A_5B_3C_2D_1E_5$. Finally, the validation experiment, conducted using spark electrical discharge machining, verifies and enhances the performance properties of ceramic composites. The gray relational rank for multi-performance enhancements of the spark eroding process also increased, from 0.7455 to 0.7782. Recent industrial applications of electrical discharge machining of molybdenum disilicide–silicon carbide composites demonstrate that the suggested method is good and provides guidance for precision manufacture.

Keywords composites, design the experiments, drilled hole accuracy, EDM, geometrical tolerances, GRA, orthogonal array

1. Introduction

High-temperature engineering applications usually prefer $MoSi_2$-SiC intermetallic/ceramic composites. Intermetallic $MoSi_2$-SiC composites have several applications due to their high strength, electrical conductivity, and hardness. These composites are frequently used in aircraft engines, combustor liners, gas turbines, and hot gas filter (Ref 1-4). It is extremely hard to machine complex forms using traditional processes, and when applied to materials of high hardness, the milling surface extensively cracks.

L. Selvarajan and **C. Arun**, Department of Mechanical Engineering, Mahendra Institute of Technology (Autonomous), Mallasamudram, Namakkal District, Tamil Nadu 637503, India; **R. Rajavel**, Department of Mechanical Engineering, Mahendra Institute of Engineering and Technology, Mallasamudram, Namakkal District, Tamil Nadu 637503, India; and **C. Raju**, Department of Mechanical Engineering, College of Engineering, Trivandrum, Kerala 695016, India. Contact e-mails: selvalakshmanan86@gmail.com and catchrajavel@gmail.com.

Abbreviations

$MoSi_2$	Molybdenum disilicide
$MoSi_2$-SiC	Molybdenum disilicide–silicon carbide
EDAX	Energy-dispersive x-ray analysis
EDM	Electrical discharge machining
EDMed	Electrical discharge machined
MRR	Material removal rate
EWR	Electrode wear rate
WR	Wear ratio
Ra	Surface roughness
ROC	Radial overcut
ROC_{Top}	Top radial overcut
ROC_{bottom}	Bottom radial overcut
θ	Taper angle
CIRTY	Circularity
CYRTY	Cylindricity
PERTY	Perpendicularity
RO	Run out
GRA	Gray relational analysis
OA	Orthogonal array
DOE	Design of experiment
S/*N* ratio	Signal-to-noise ratio
GD & T	Geometrical dimensioning & tolerances
SEM	Scanning electron microscope
Si_3N_4-TiN	Silicon nitride-titanium nitride
VMM	Video measuring machine
MPa	Mega Pascal
μm	Micrometer
ANOVA	Analysis of variance

Published online: 11 December 2023

In addition, it produces a built-up edge that is difficult to machine. This causes the cutting tool to wear out more quickly during machining, demanding the purchase of a more expensive tool. Ceramic composites can currently be machined using the EDM process with assurance. Due to its reduced cost and increased practicality, electrical discharge machining (EDM) is recommended for such research. EDM is a non-traditional machining process that ensures acceptable dimensional precision in electrically conducting materials despite their high thermal and compressive strengths. The Si_3N_4 matrix is improved with the use of electron-transmitting particles like ZrB_2, TiN, TiC, and TiB_2. EDM can mill whatever conducts electricity, regardless of its form, corrosion resistance, hardness, or high wear resistance (Ref 5-8). Selvarajan et al. (Ref 9) investigated the application of spark EDM for machining electrically conductive ceramic composites.

Ming et al. (Ref 10) investigated ceramic composites and determined that they maintained oxidation resistance when they were heated to high temperatures, which makes them an intriguing opportunity to be utilized as a high-temperature structural material. Aerospace structural applications are an excellent fit for the mechanical, physical, and thermal properties of composites, as discovered by Jiang et al. and Zhang et al. (Ref 11, 12). Because of their potential effectiveness in oxidizing and under extreme conditions, molybdenum disilicide composites have been explored through the use of a broad range of reinforcing approaches, including the inclusion of molybdenum, niobium, tantalum, and niobium–aluminum–titanium alloy as fibers and lamellae. All-silicon carbide and all-molybdenum-disilicide composites are only two examples of the synthetic materials obtainable.

According to Selvarajan et al. (Ref 13), this material is ideal for high-temperature structural applications due to its high melting point (2020 °C), outstanding oxidation resistance, low density (6.4 g/cm^3) compared to super alloys, and thermodynamic compatibility with a wide range of ceramic reinforcements. By integrating $MoSi_2$ doped with SiC particles using hot-pressing processes, Selvarajan et al. (Ref 14) demonstrated that these materials are electrically conductive ceramic-based composites having potential applications in the aerospace industry. This research aims to identify the optimum electrode materials for electrical discharge machining (EDM) of conductive composites. Based on the work of Selvarajan et al. (Ref 15), because of their high material reduction ratio (MRR), high geometrical tolerance (GTR), and affordable cost, copper electrodes came highly recommended in the author's electrical discharge machining research. Copper electrodes have been demonstrated to be more beneficial for high metal removal rates in EDMed ceramic composites, according to the research.

Alduroobi et al. (Ref 16) carried out a design of experiments (DOE) using a Taguchi orthogonal array to analyze the effects of process factors on the material removal rate (MRR), electrode wear rate (EWR), and other performance parameters of an ALSI 1045 steel work piece. The author shows the Taguchi method as a potential approach to improving multi-response features.

To enhance the EDM procedure, Chaudhari et al. (Ref 17) employed a gray relational analysis technique. The gray theory could provide a response in situations when the model is insufficient or where there is a lack of information. It works well with a variety of inputs and data types, especially those that include both continuous and discrete data. In order to improve the Taguchi and gray relationship analysis activities, several different forms of responses were utilized. The Taguchi orthogonal array is employed to generate trials for gray relational analysis for process optimization. The most important aspect, the impact of process parameters on the EDMed method, was investigated as well, utilizing analysis of variance (Ref 18, 19). The EDM process has a requirement for an accurate form tolerance for the holes it creates. To improve the hole form tolerances attained by electric discharge machining, this process must be enhanced. Geometric tolerance for Si_3N_4 composites was studied by Selvarajan et al. (Ref 20).

The purpose of geometric dimensioning and tolerance (GD&T) is to specify the required geometric dimensions and tolerances for parts and assemblies. Functional criteria like accessibility for assembly with the intended counterpart(s) and appropriate functioning of the mechanical system are included in this research, but the analysis of geometrical faults is the primary focus. Few investigations of geometrical errors in Spark EDM of ceramic composites have been reported in the literature. EDM's impact on geometrical flaws, including circularity, cylindricality, and perpendicularity, has not been empirically studied. Due to their significance in the electric discharging process, geometrical errors have a significant impact on the quality of the responses.

The thermal degradation, collapse of material, and unevenness of the machined surface resulting in the presence of major and minor cracks and craters (such as deep craters and swallow craters) during the manufacturing or machining of conductive ceramic composites for use in high-temperature environments are all contributors to poor surface quality. Maintaining rigorous measures of quality control is essential for preventing such issues. Thus, any microstructural faults that may affect the product's lifetime must be investigated and analyzed (Ref 21, 22).

Geometric tolerances provide for the most efficient and effective communication of design information. To achieve this goal, designers and manufacturers have to be able to specify and analyze the specified characteristics and tolerances. This is helpful in ensuring that the minimum amounts of configuration requirement have been satisfied. The industry goal is to mass-produce the specified components at a reasonable cost, all the while embracing the pre-designed protections that ensure precise size. Incorporating tolerances into geometry is essential for precision. One may assume that geometrical tolerance is one of the most important factors to consider while milling ceramic composites (Ref 23-25).

The results of this study demonstrate that there is a lack of knowledge with regard to the limitations of the MRR, the degree of wear, and the geometrical tolerances of the EDM process when it comes to machining ceramic composite materials. Also investigate the impact of pores, craters, and thermal spalling on the performance of $MoSi_2$-SiC composites (Ref 14, 25-27). In order to search for defects such as chips, cracks, globules of varying sizes, debris, craters, and pores, the team utilized SEM equipment analysis with an EDAX report of the machined surface. By analyzing the surface textures of the machined surfaces of the work piece with SEM images, we expected that the input process parameters would be accountable for these modifications (Ref 20, 28).

This research addresses the knowledge gap in geometrical tolerances, machining wear, and material removal rate (MRR) of ceramic composite materials, specifically $MoSi_2$-SiC composites, during electrical discharge machining (EDM). The study explores the impact of surface flaws like cracks and craters on the composite's overall performance.

The related literature review reveals limited work on EDM for ceramic composites like $MoSi_2$-SiC, with only a few studies

considering various performance measures such as material removal rate, top radial overcut, wear ratio, surface roughness, tool wear rate, cylindricity, bottom radial overcut, taper angle, run out, perpendicularity, and circularity. The geometrical tolerance effects of the EDM process on $MoSi_2$-SiC composites are inadequately studied, and there is a lack of research using gray analysis to optimize EDM process parameters for ceramic composites.

The study applies the GRA approach and the ANOVA method to identify optimal parameters for enhancing geometrical tolerances in $MoSi_2$-SiC composites. Experimental work, employing scanning electron microscopy (SEM) for topography analysis, is carried out to investigate the impact of EDM on the composites. The process parameters, including current, sparking ON time, sparking OFF time, spark gap voltage, and flushing pressure, are optimized using material removal rate, bottom radial overcut, wear ratio, top radial overcut, circularity, tool wear rate, cylindricity, surface roughness, perpendicularity, and run out as criteria.

Overall, the research aims to quantify geometrical defects and performance factors such as productivity, dimensional deviation, and surface roughness in EDM of $MoSi_2$-SiC composites. The final confirmation experiment assesses whether the process parameter adjustments result in desired improvements in material removal rate and wear ratio, while reducing tool wear rate, cylindricity, radial overcut, circularity, perpendicularity, and run out.

2. Experimental Design and Methodology

Taguchi experiments are designed to reduce the time and effort spent testing and analyzing variables. In this research, $MoSi_2$-SiC was employed as a specimen material. $MoSi_2$-SiC materials are electrical conductivity 0.00143 Ωm, thermal conductivity 42 W/mK, hardness 11.5 GPa, coefficient of thermal expansion 8.2 K^{-1}, flextural strength 338 MPa. A heat-pressed $MoSi_2$-SiC ceramic composite is part of the work. To generate a high MRR, a copper-based electrode of Cu composition was used as a rod 5 mm in diameter and 20 mm in length. A fresh set of electrodes is used for every experiment. Figure 1 shows the EDM machine in operation, and the electrodes after an EDM operation are shown in Fig. 2.

To calculate the MRR, we compared the pre- and post-spark EDM weights of the machined $MoSi_2$-SiC. Machined electrodes and $MoSi_2$-SiC were both weighed to an accuracy of 0.001 g using an electronic balance. The EDM machine was used to conduct the experiments as planned. The amount of machining time spent on each experiment was noted. Table 1 shows the machining settings, and Table 2 shows the response parameters for the experimental results. Processing circumstances and response parameters interact, as shown in Fig. 3.

The MRR, was determined using Eq 1,

The metal removal rate (MRR) has been calculated for each experiment using the following Eq 1:

$$\mathrm{MRR}\ (\mathrm{g/min}) = \frac{w_{wb} - w_{wa}}{t} \quad \text{(Eq 1)}$$

The tool wear rate (TWR) has been calculated with Eq 2.

$$\mathrm{TWR}\ (\mathrm{g/min}) = \frac{W_{tb} - W_{ta}}{t} \quad \text{(Eq 2)}$$

Fig. 1 Spark EDM machine (OSCARMAX)

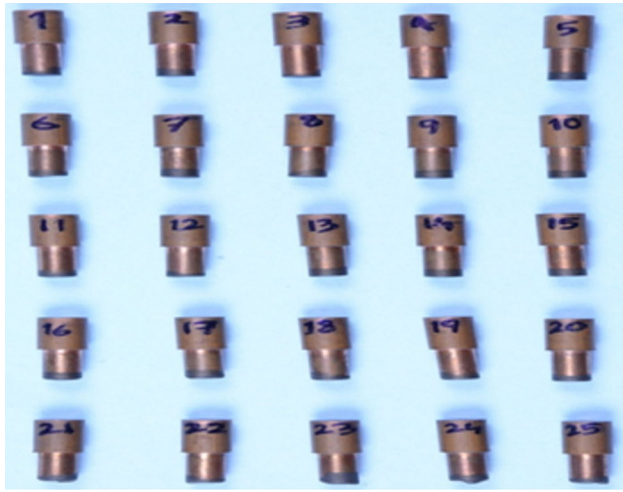

Fig. 2 Machined electrodes

The wear ratio (WR) has been determined as shown in Eq 3.

$$\mathrm{WR} = \frac{\mathrm{MRR}}{\mathrm{EWR}} \quad \text{(Eq 3)}$$

The radial overcut has been determined as shown in Eq 4 and 5.

Radial overcut,

$$\mathrm{ROC_{top}} = \left\{\frac{D_{\mathrm{top}} - D_{\mathrm{electrode}}}{2}\right\} \quad \text{(Eq 4)}$$

$$\mathrm{ROC_{bottom}} = \left\{\frac{D_{\mathrm{bottom}} - D_{\mathrm{electrode}}}{2}\right\} \quad \text{(Eq 5)}$$

Taper angles in degrees have been determined as shown in Eq 6.

$$\theta = \tan^{-1}\left\{\frac{D_{\mathrm{top}} - D_{\mathrm{bottom}}}{2t}\right\} \quad \text{(Eq 6)}$$

Weighing Scale

With the help of a precise scale, we were able to figure out how much the tool and the workpiece weighed together. This

Table 1 shows the machining settings

Factor	Parameter	Units	Stage 1	Stage 2	Stage 3	Stage 4	Stage 5
A	'Current'	A	2	3	4	5	6
B	'Sparking ON time'	μs	6	7	8	9	10
C	'Sparking OFF time'	μs	3	4	5	6	7
D	'Spark Gap voltage'	V	35	37.5	40	42.5	45
E	'Flushing pressure'	kg/cm^2	15	16	17	18	19

Table 2 shows the response parameters for the experimental results

S. No.	MRR gm/min	EWR gm/min	WR %	Ra μm	ROC_{TOP} mm	ROC_{BOT} mm	θ degree	CIRTY mm	CYRTY mm	PERTY mm	RO Mm
1	0.01275	0.00115	11.0400	0.255	0.0655	0.0185	1.3462	0.029	0.025	0.015	0.095
2	0.00786	0.00042	18.6000	0.224	0.1080	0.0350	2.0904	0.054	0.055	0.019	0.083
3	0.01850	0.00147	12.5455	0.330	0.0730	0.0075	1.8758	0.068	0.063	0.035	0.189
4	0.02175	0.00169	12.8571	0.528	0.0805	0.0020	2.2477	0.075	0.073	0.035	0.136
5	0.01159	0.00059	19.6000	0.547	0.0740	0.0345	1.1314	0.055	0.059	0.019	0.087
6	− 0.00225	0.00283	− 0.7941	0.497	0.0875	0.0675	0.5729	0.106	0.070	0.019	0.112
7	0.03515	0.00404	8.6933	0.347	0.0755	− 0.0155	2.6052	0.049	0.050	0.019	0.130
8	0.02441	0.00373	6.5435	0.355	0.0935	− 0.0060	2.8481	0.068	0.057	0.017	0.098
9	0.02121	0.00297	7.1500	0.264	0.0750	− 0.0495	3.5621	0.057	0.058	0.011	0.058
10	0.01762	0.00145	12.1250	0.547	0.0870	0.0300	1.6325	0.045	0.049	0.012	0.041
11	0.01722	0.00405	4.2576	0.488	0.0820	− 0.0535	3.8759	0.059	0.061	0.004	0.037
12	0.02025	0.00675	3.0000	0.350	0.1180	0.0490	1.9759	0.105	0.087	0.005	0.032
13	0.01488	0.00308	4.8281	0.345	0.1120	0.0200	2.6337	0.121	0.194	0.032	0.217
14	0.02833	0.00315	9.0000	0.428	0.1405	− 0.0040	4.1324	0.124	0.097	0.022	0.096
15	0.02525	0.00167	15.1053	0.997	0.1155	0.0380	2.2191	0.167	0.115	0.036	0.148
16	0.00558	0.00098	5.6837	0.563	0.0790	− 0.0235	2.9338	0.045	0.058	0.016	0.068
17	− 0.05595	0.01302	− 4.2963	0.366	0.0865	− 0.1575	6.9557	0.059	0.079	0.009	0.046
18	0.04772	0.00942	5.0678	0.349	0.0880	− 0.2790	10.3981	0.073	0.055	0.016	0.066
19	0.04475	0.00799	5.6000	0.227	0.0910	− 0.1370	6.5036	0.057	0.059	0.010	0.056
20	0.03978	0.00779	5.1053	0.365	0.0950	− 0.1215	6.1782	0.061	0.038	0.008	0.063
21	0.01974	0.01451	1.3604	0.493	0.1300	− 0.0245	4.4173	0.060	0.067	0.016	0.052
22	0.03374	0.01359	2.4831	0.512	0.1160	− 0.0340	4.2892	0.132	0.090	0.012	0.088
23	0.02748	0.01047	2.6250	0.339	0.1450	0.0930	6.7863	0.178	0.157	0.029	0.163
24	0.02569	0.01523	1.6867	0.376	0.0930	− 0.1330	6.4471	0.058	0.043	0.014	0.086
25	0.02995	0.01940	1.5435	0.443	0.1040	0.0360	1.9473	0.083	0.058	0.018	0.086

device can measure to within 0.001 gramme, with a maximum capacity of 300 g. The CG 203 is made by Citizen Scale (I) Pvt. Ltd. in Mumbai.

Machines and Tools

The OSCARMAX Spark EDM machine was used to machine the specimens for the experiments. In Thailand's die-sinking SD325-ZNC model in Fig. 4, we see the finished product of the machining process.

In Fig. 5, we see the results of hole entry measurements taken using VMM and ARCH software on $MoSi_2$-SiC composites.

Roughness was measured to within 5.5 microns using specialized equipment.

As shown in Fig. 6, geometrical errors were quantified with the use of a coordinate measuring machine (CMM) and the universal CMM software GEOMET.

Improving productivity, dimensional deviation, and surface roughness by adjusting EDM process parameters is discussed in this article.

2.1 Main Effect Plot for Output Parameters on $MoSi_2$-SiC Composite

2.1.1 Material Removal Rate. The main effects plot shows in Fig. 7 that the maximum MRR is achieved with the following parameters: current level 5, pulse on time level 4, pulse off time level 1, dielectric pressure level 4, spark gap voltage 4, and dielectric pressure level 4.

The mechanism behind this can be explained as follows:

- Current: A higher MRR can be achieved by increasing the current level, as this provides more energy to melt and evaporate the material.
- Pulse on time: Allowing the electrical discharge to go on for a longer time will increase the peak power density, which in turn can increase the MRR.
- Pulse off time: A higher MRR may be achieved by decreasing the pulse off time and thus increasing the duration of the electrical discharge.

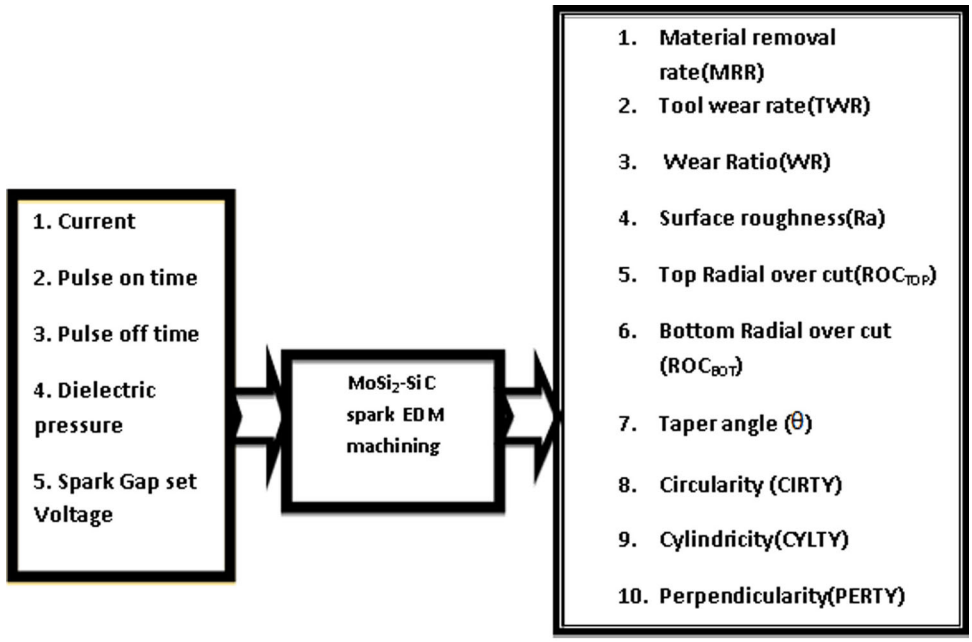

Fig. 3 Processing circumstances and response parameters interact

Fig. 4 Workpiece for 25 experiments on a machine

- Dielectric pressure: Increasing the dielectric pressure can improve MRR by making the dielectric fluid flush more effectively and getting rid of the debris more promptly.
- Spark gap voltage: Increasing the voltage across the spark gap can boost the energy density of the electrical discharge, which in turn can improve the MRR.

2.1.2 Electrode Wear Rate. According to the main effects shown in Fig. 8, the minimal EWR is achieved with a current of 2 A, a pulse on time of 6 s, a pulse off time of 4 s, a dielectric pressure of 16 kg/cm^2, and a spark gap voltage of 45 V.

The mechanism behind this can be explained as follows:

- Current: Less current flowing between the workpiece and the tool reduces electrode wear and the electrical work rate (EWR).
- Pulse on time: Since the dielectric fluid has less time to flush out the debris during a shorter pulse on time, the electrode may experience less erosion and consequently have a lower EWR.
- Pulse off time: A longer pulse off time means that the electrical discharge lasts for a longer time, which can lead to more efficient material removal and less electrode wear, resulting in a lower EWR.
- Dielectric pressure: When the dielectric pressure is low, the flushing effect of the dielectric fluid may be lessened, so it has less of an effect on the electrode and the EWR goes down.
- Spark gap voltage: With a higher spark gap voltage, the electrical discharge can have more energy, resulting in more effective material removal and less electrode wear, and thus a lower EWR.

2.1.3 Surface Roughness. As shown in the main effects Fig. 9, the minimum SR is achieved under conditions where the current is at level 4, the pulse on time is at level 3, the pulse off time is at level 3, the dielectric pressure is at level 1, and the spark gap voltage is at level 2. The mechanism behind this can be explained as follows:

- Current: A higher current level indicates that more electrical energy passes into the workpiece and the tool, which results in more effective material removal and smoother surfaces, resulting in reduced SR.
- Pulse off time: The melting and vaporization of the material may be minimized and the surface roughness reduced by using a shorter pulse off time during the electrical discharge.
- Pulse on time: A longer pulse on time implies that there is more time for the dielectric fluid to flush out the debris,

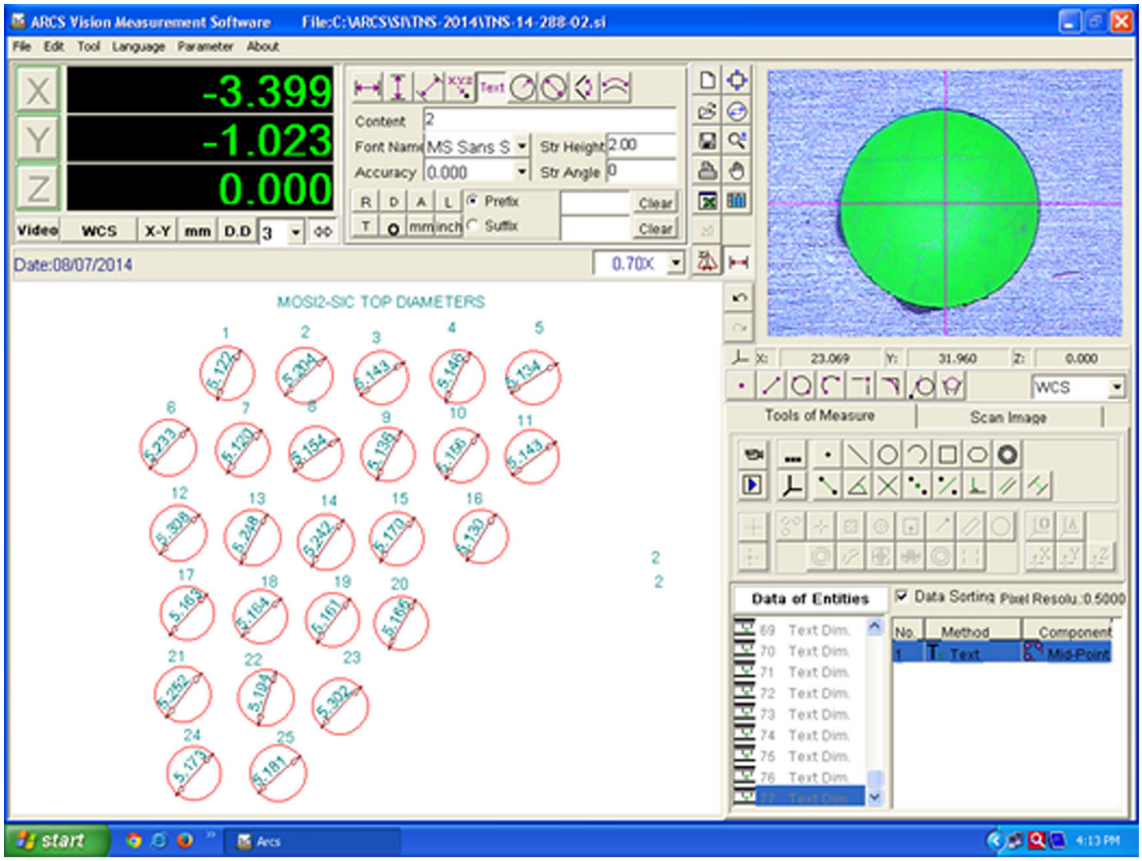

Fig. 5 Hole entrance diameter of the $MoSi_2$-SiC composites using VMM and ARCH software

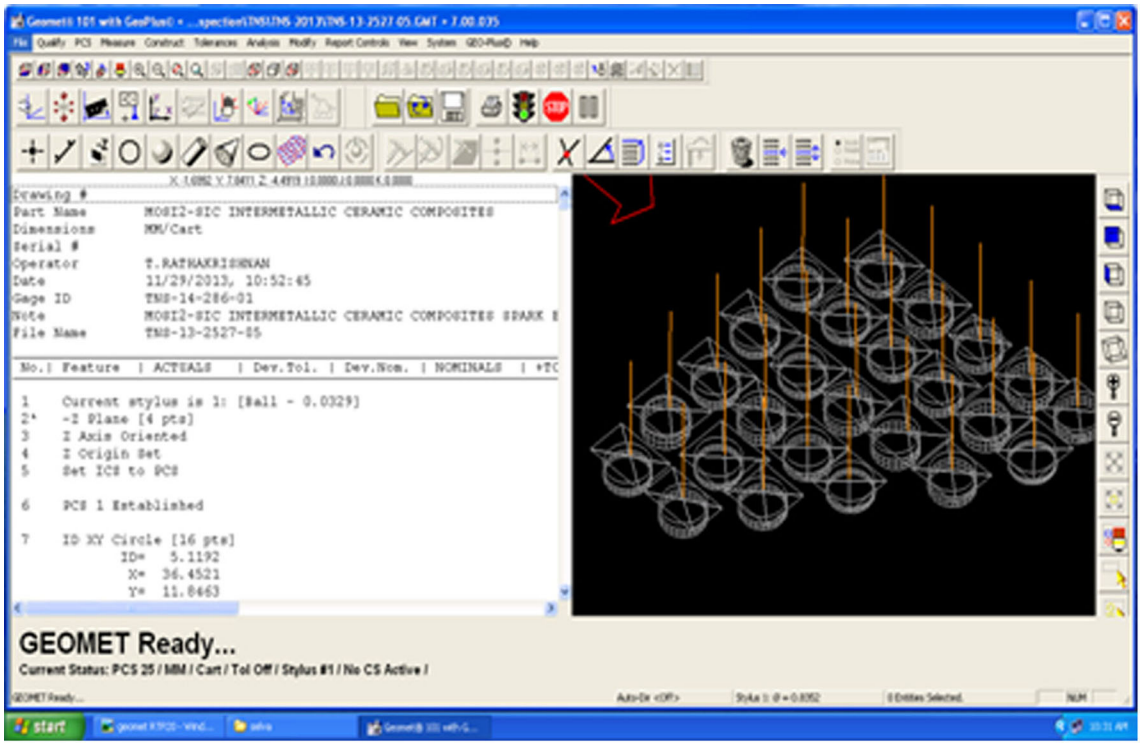

Fig. 6 GEOMET universal CMM software is used to measure geometrical tolerance

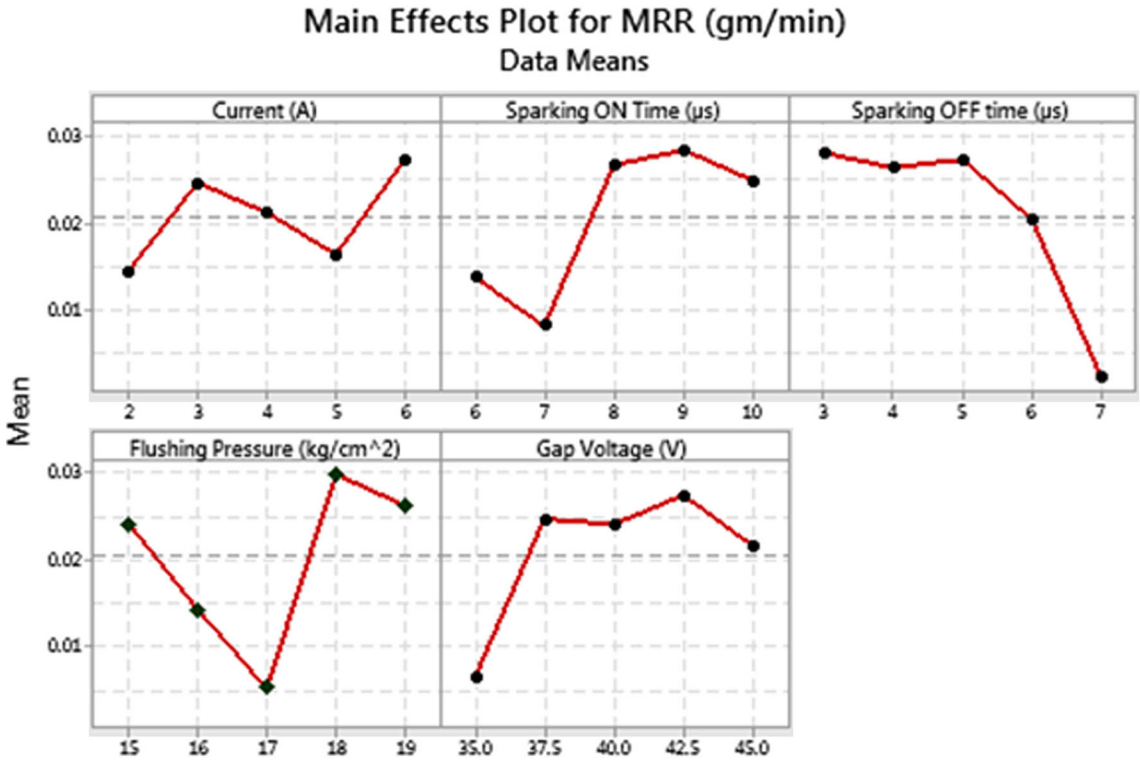

Fig. 7 Mean effect plot for MRR

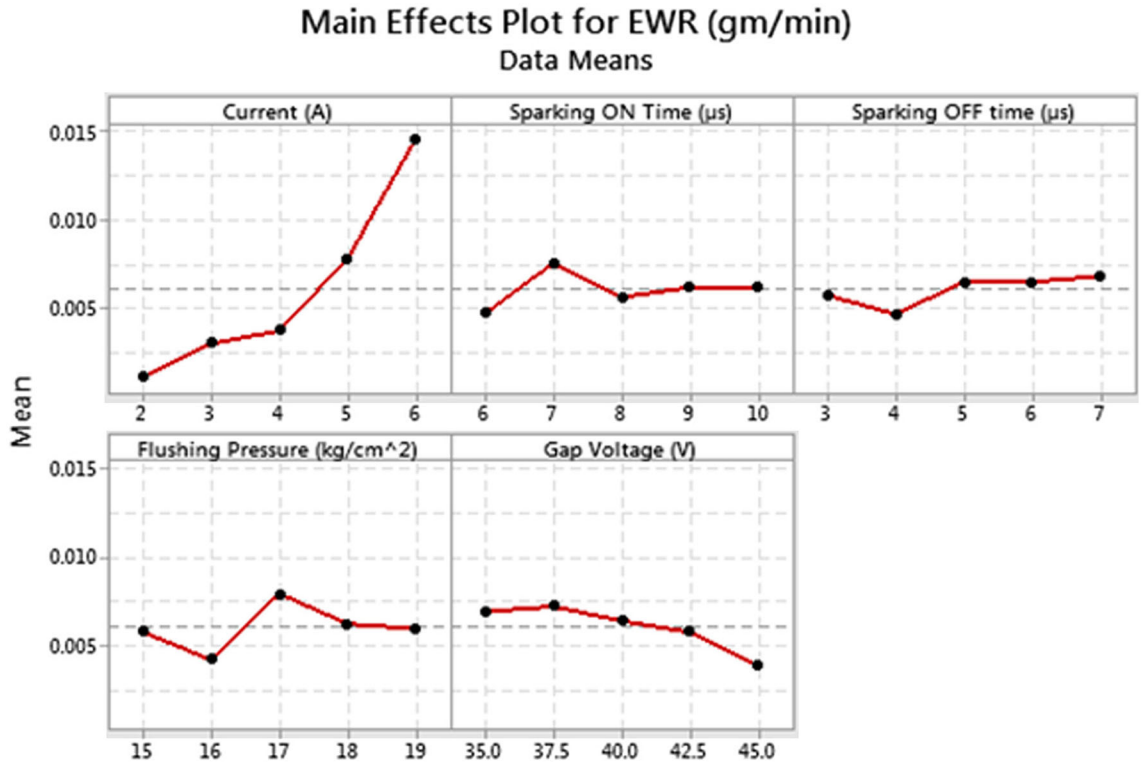

Fig. 8 Mean effect plot for EWR

which may minimize the surface roughness by eliminating the debris from the machining zone and leaving smoother surfaces.

- Dielectric pressure: Reduced turbulence and effects on the machined surface from the dielectric fluid flushing operation may lead to lower SR and smoother surfaces when the dielectric pressure is lowered.

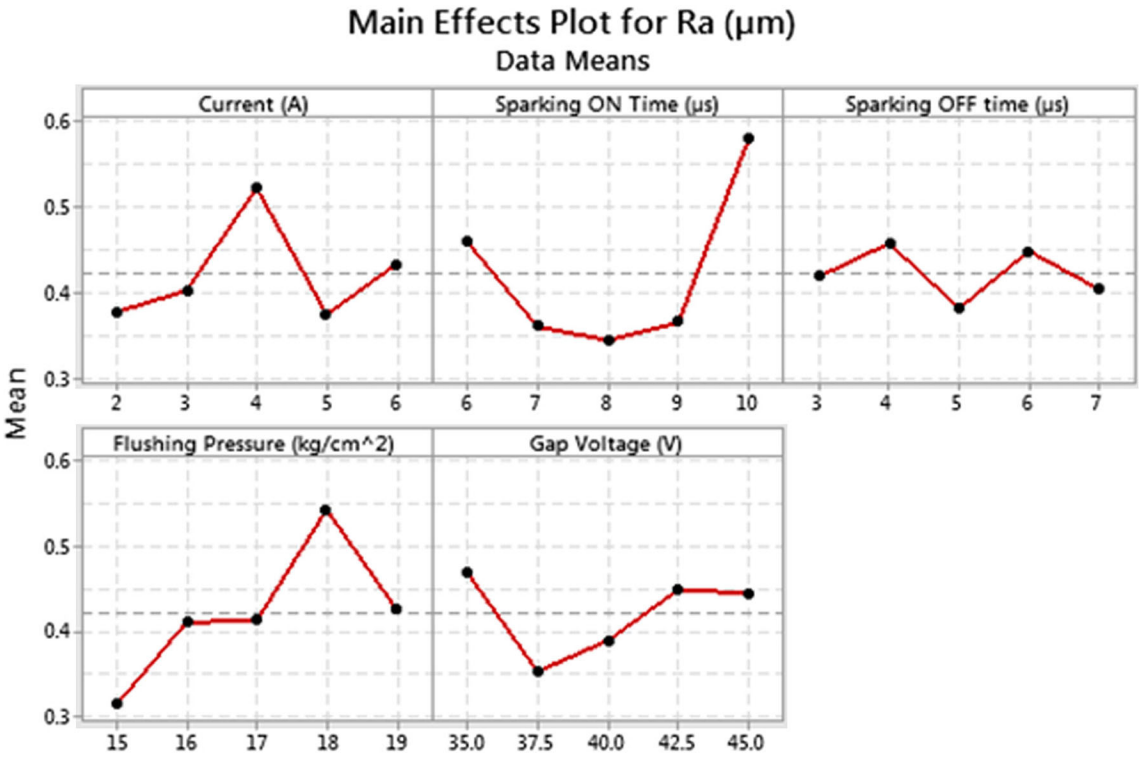

Fig. 9 Mean effect plot for surface roughness

- Spark gap voltage: An improvement in surface smoothness and SR can be achieved by using a spark gap voltage that is lower than that required for melting and vaporization to occur.

2.1.4 Top Radial Overcut. Using these particular values for the parameters shown in Fig. 10, we can explain how we get the smallest possible top radial overcut:

- Current: The current level of 2 A guarantees that the electric discharge is steady and uniform, which stops excessive material removal and, as a result, reduces the amount of top radial overcut that occurs.
- Pulse off time: A pulse-off time of 5 s is enough to start material removal and make a strong spark. This makes sure that enough material is removed but not too much, which again helps to reduce top radial overcut.
- Pulse on time: A pulse on time of 6 μs ensures that the discharge stops quickly, which minimizes the chances of overcutting.
- Dielectric pressure: The high dielectric pressure level of 19 kg/cm^2 creates a uniform electric field around the electrode, which ensures that material removal is uniform and top radial overcut is minimized.
- Spark gap voltage: The low spark gap voltage level of 35 Volts ensures that the discharge is not too strong, which prevents excessive material removal and minimizes top radial overcut.

2.1.5 Bottom Radial Overcut. With these precise parameters shown in Fig. 11, the technique for achieving minimal bottom radial overcut is as follows:

- Current: Bottom radial overcut is reduced because the 2 A current level guarantees a steady and uniform electric discharge, which avoids the removal of too much material.
- Pulse off time: For effective material removal, a pulse off time of about 6 s is all that is needed to generate a powerful spark. This again aids in reducing bottom radial overcut by ensuring effective, but not excessive, material removal.
- Pulse on time: Overcutting is prevented by a 6 s pulse on time, during which the discharge is abruptly terminated.
- Dielectric pressure: Because of the homogenous electric field produced by the high dielectric pressure level of 16 kg/cm^2, material removal is consistent and bottom radial overcut is kept to a minimum.
- Spark gap voltage: With a 45 V spark gap voltage, bottom radial overcut is kept to a minimum and excessive material removal is avoided.

2.1.6 Taper Angle. The primary impact, Fig. 12, revealed that certain values for the input process parameters resulted in the smallest possible taper angle. For instance, cutting with a current of 2 A yielded the smallest taper angle, suggesting that lower currents allow for more accurate material removal or less deformation of the shape being cut. Similarly, the smallest taper angle was achieved with a pulse on time of 6 to 10 s, which might mean that longer pulses are superior for material removal or smoothing down the surface. Although the precise impacts of the other input parameters on the EDM process and material removal are context-dependent, they are likely to be comparable.

2.1.7 Circularity. This could be because the input process parameters, as shown in Fig. 13, at these levels give the electro-discharge machining (EDM) process the best conditions

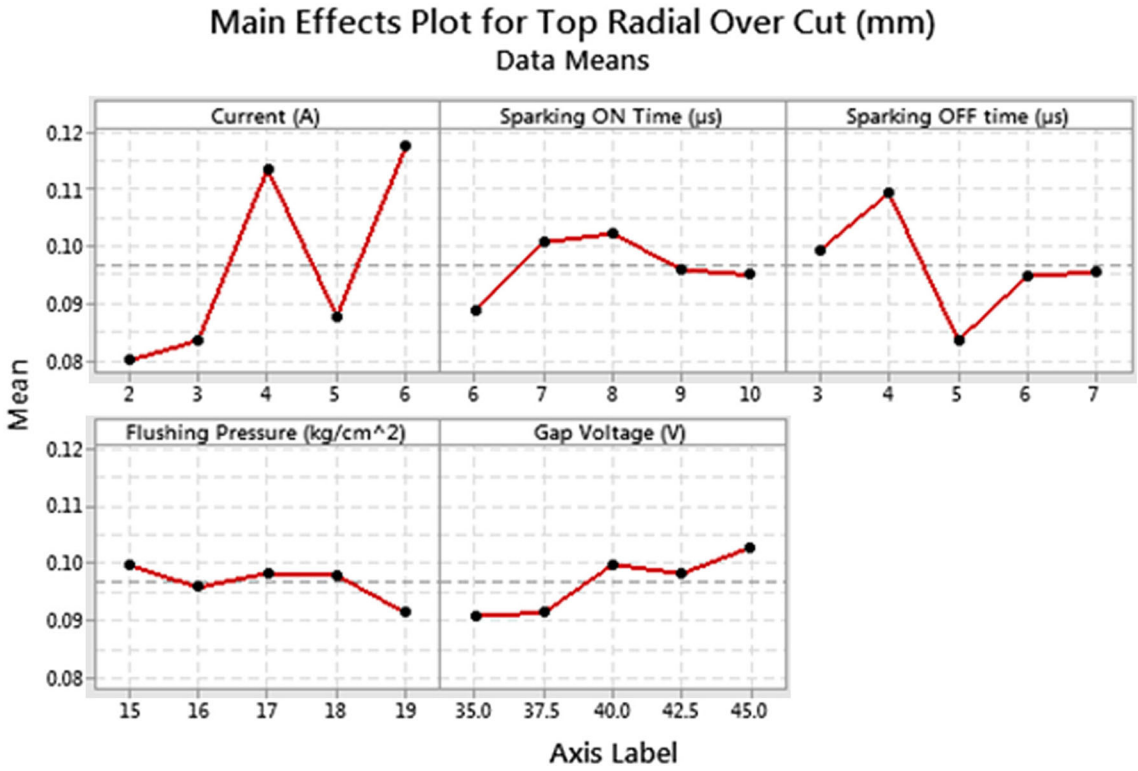

Fig. 10 Mean effect plot for top radial overcut

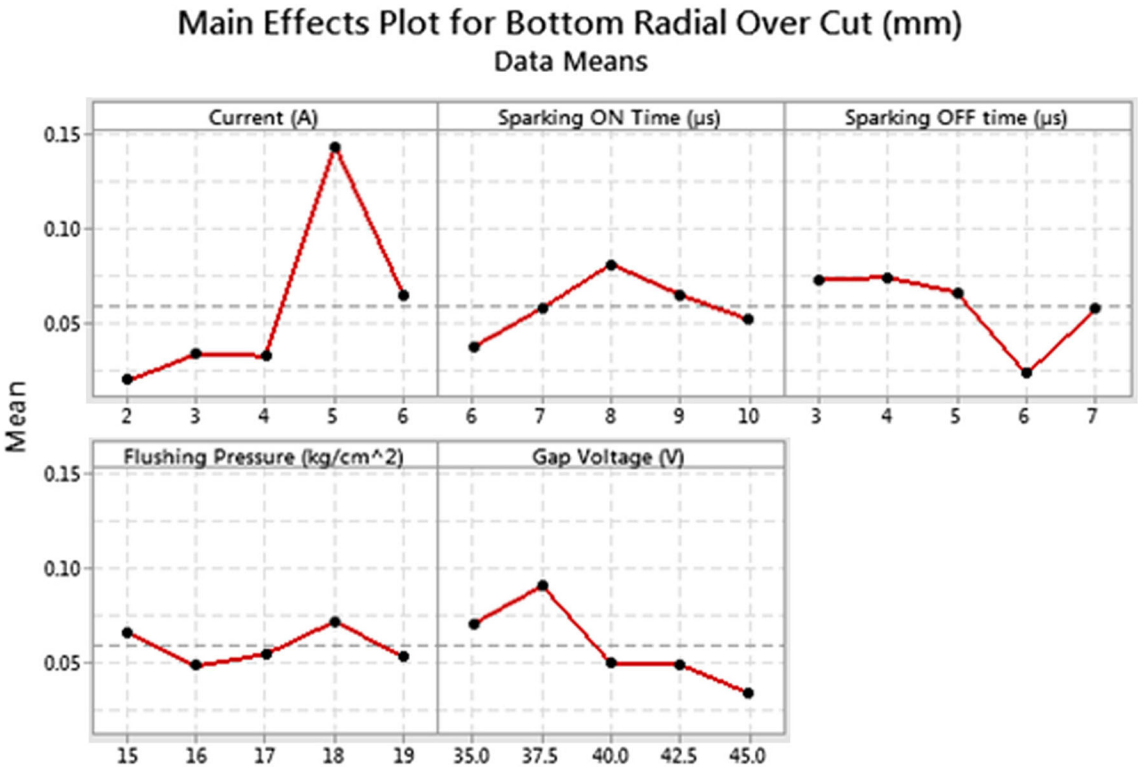

Fig. 11 Mean effect plot for bottom radial overcut

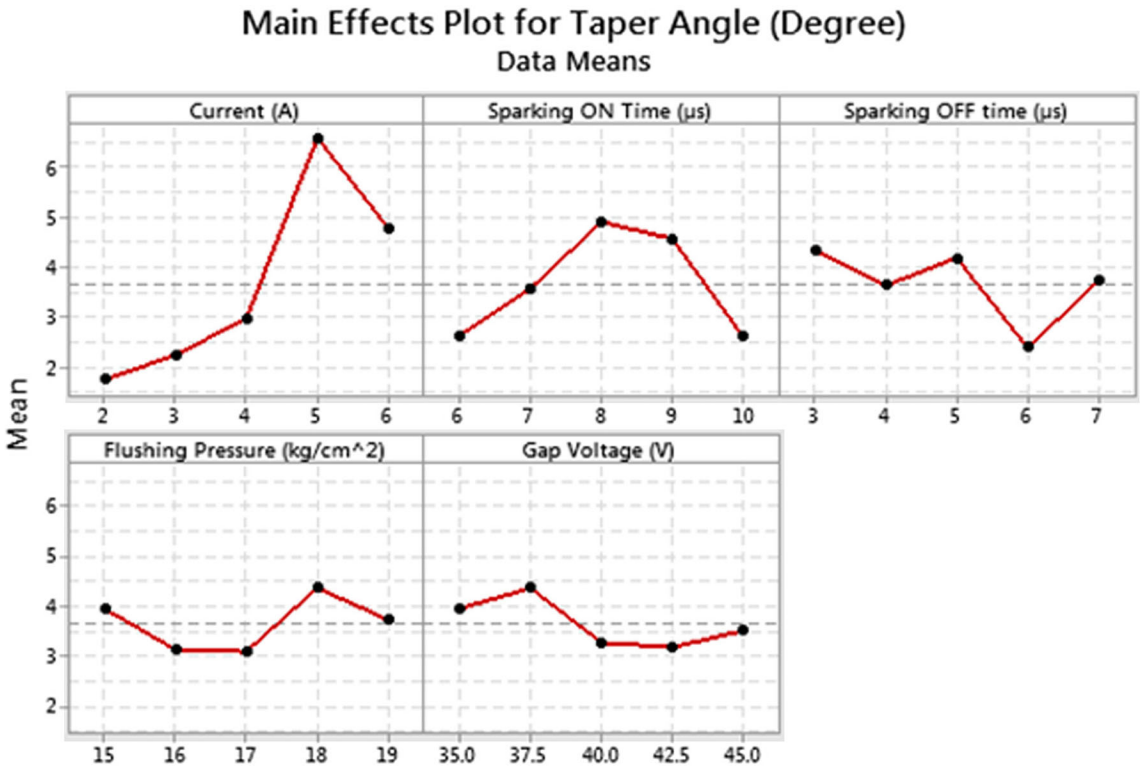

Fig. 12 Mean effect plot for taper angle

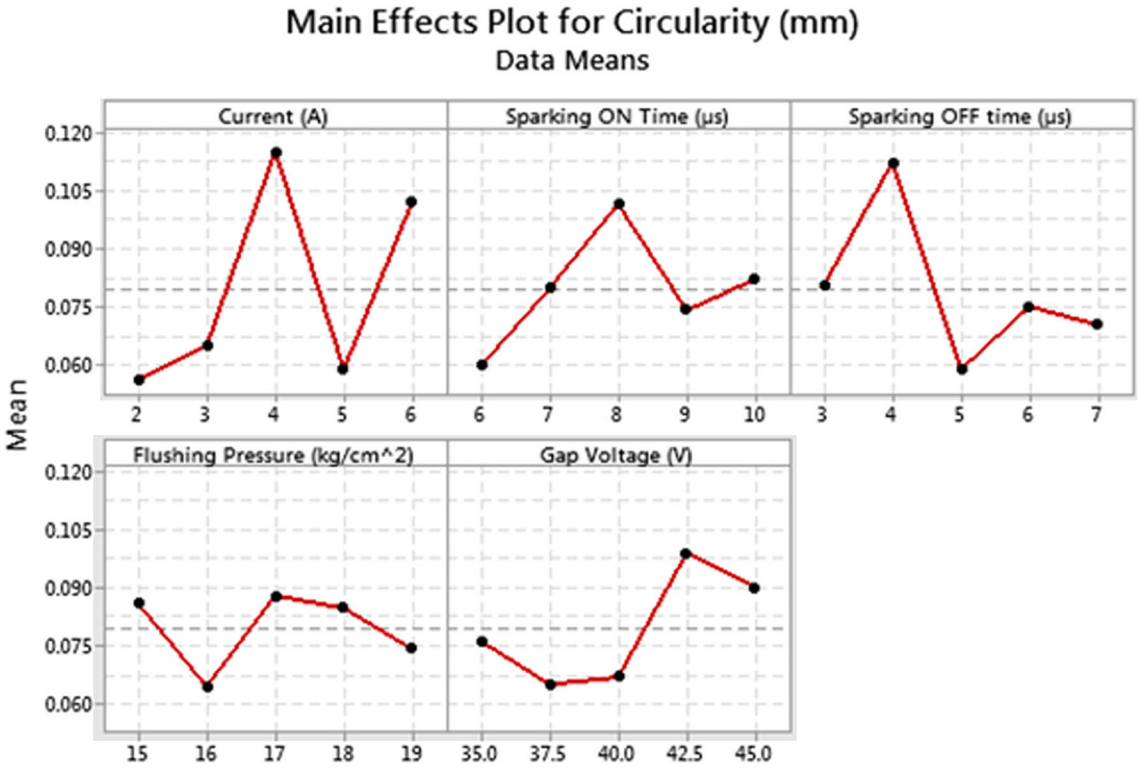

Fig. 13 Mean effect plot for circularity

possible. Electrical discharge machining (EDM) removes material from a workpiece by using a dielectric fluid and an electrode on the tool. The degree to which a machined feature is round depends on many things, such as the shape of the electrode, the machining conditions, and the quality of the material.

The shape and size of the electrode affect both the spark discharge and the rate at which material is removed. This, in turn, depends on the exact combination of input process parameters that leads to the least circularity. For instance, greater heat may be generated at the higher current level (4 or 5 A), which may facilitate the removal of material. The spark discharge may be managed and electrode wear reduced by selecting the appropriate pulse on (level 1-6) and off (level 3-5) times. Level 2 (16 kg/cm^2) of dielectric pressure is ideal for minimizing arcing and maximizing spark discharge efficiency. Last but not least, the appropriate spark gap voltage (level 2 of 37.5 V) may aid in ensuring steady spark discharges and enhancing the pace at which material is removed.

2.1.8 Cylindricity. The mean effect plot for cylindricity is shown in Fig. 14,

- Current: Since it offers adequate energy for the machining process to remove material without creating undue deformation or distortion of the workpiece, the current level of 2A may be appropriate for attaining minimal cylindricity.
- Pulse off time: At level 3, the pulse off time is 5 s, which may be long enough to transfer enough energy to the workpiece to remove material yet short enough to minimize the length of the spark discharge to minimize the amount of heat created.
- Pulse on time: There may be enough time for the discharge to die out and the workpiece to cool down before the next spark discharge occurs with a pulse on time of 6 s at level 1.

2.1.9 Perpendicularity. The mean effect plot for perpendicularity is shown in Fig. 15.

- Perpendicularity is improved by the current. While moving from current level 1 to current level 2, the perpendicularity likewise rises.
- The perpendicularity suffers when the Pulse is turned off. Perpendicularity weakens when Pulse off time is reduced from level 2 to level 1.
- Perpendicularity is improved by keeping the pulse on time. The perpendicularity rises from level 1 to level 2 as the Pulse on time rises from 2 to 3.
- The dielectric pressure causes a decrease in perpendicularity. From level 4 to level 5, the dielectric pressure drops, and with it, the perpendicularity.
- Perpendicularity degrades as the spark gap voltage increases. Perpendicularity is reduced from level 1 to level 2 when the spark gap voltage is lowered.

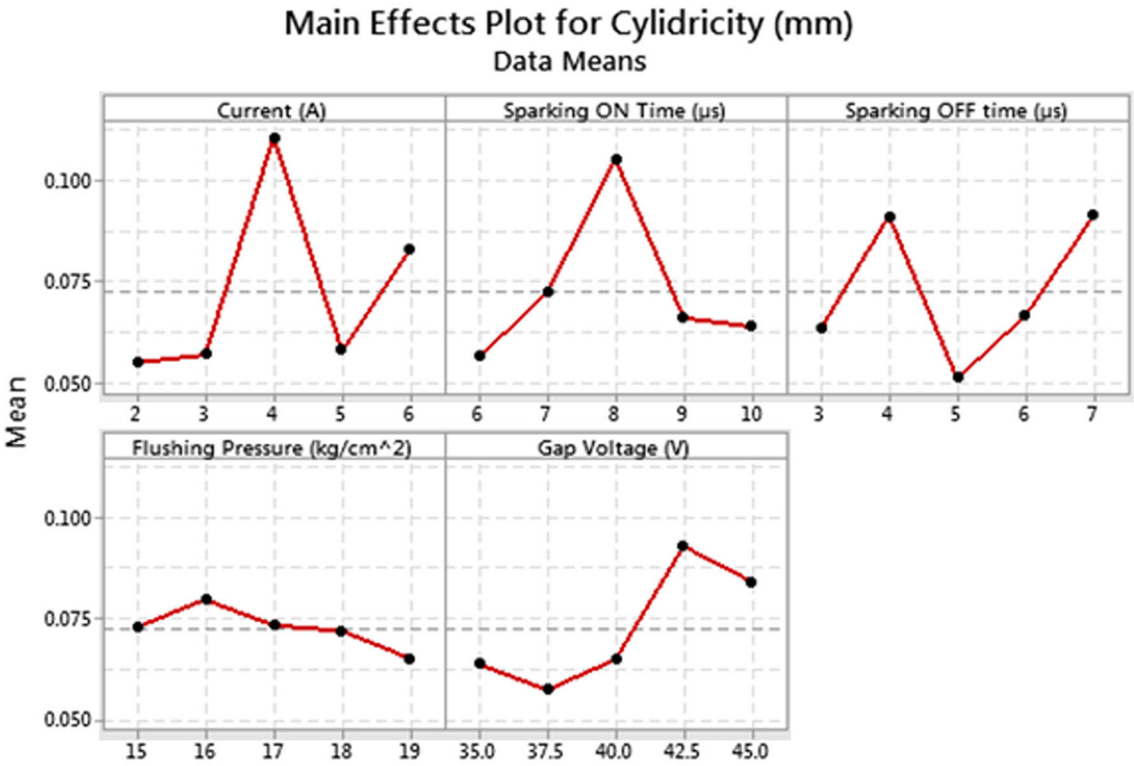

Fig. 14 Mean effect plot for cylindricity

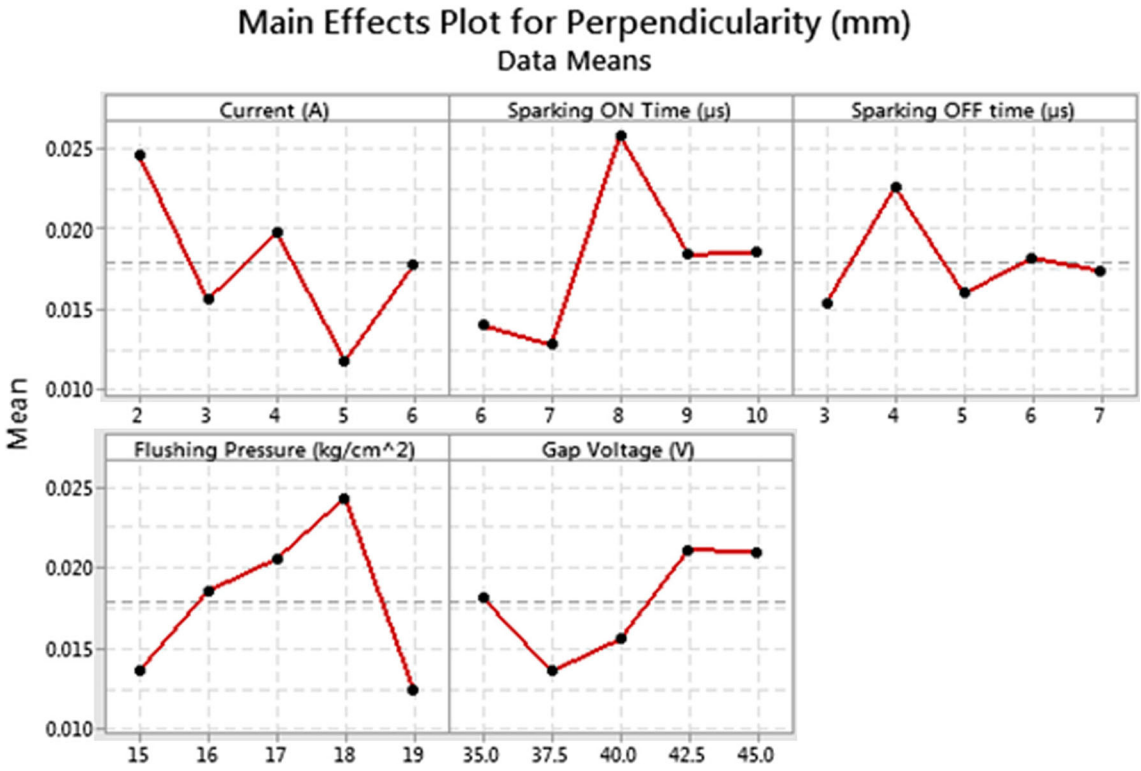

Fig. 15 Mean effect plot for perpendicularity

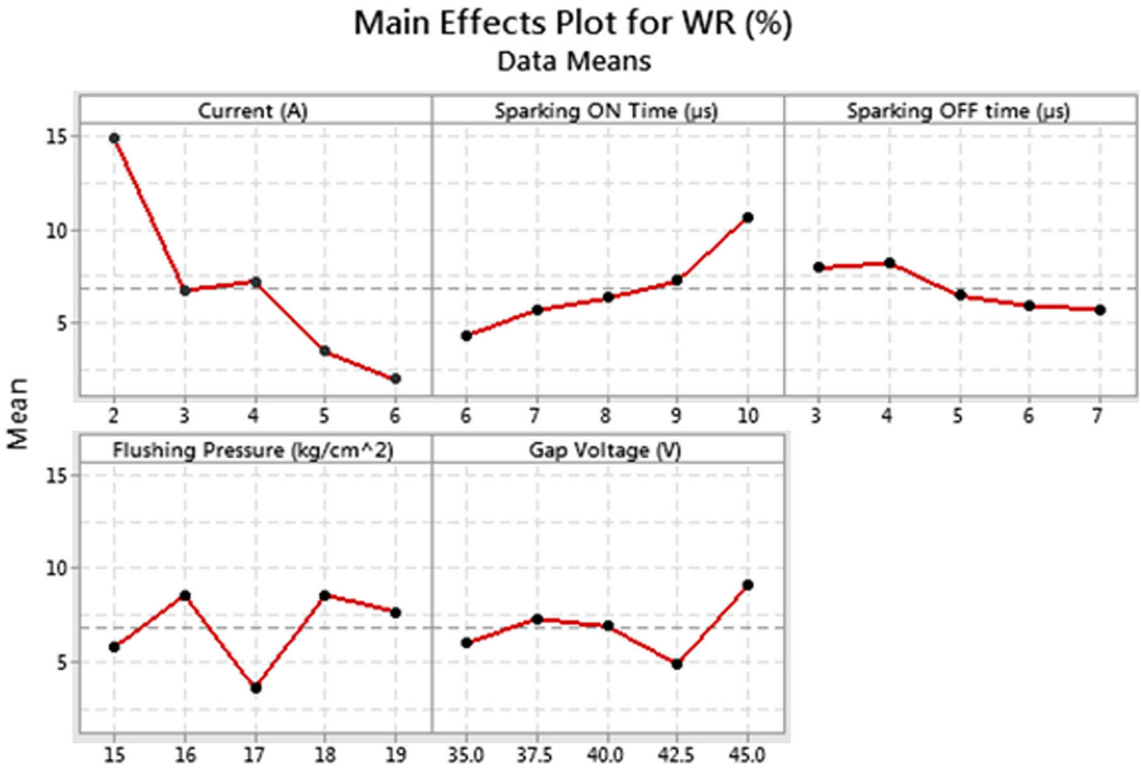

Fig. 16 Mean effect plot for wear ratio

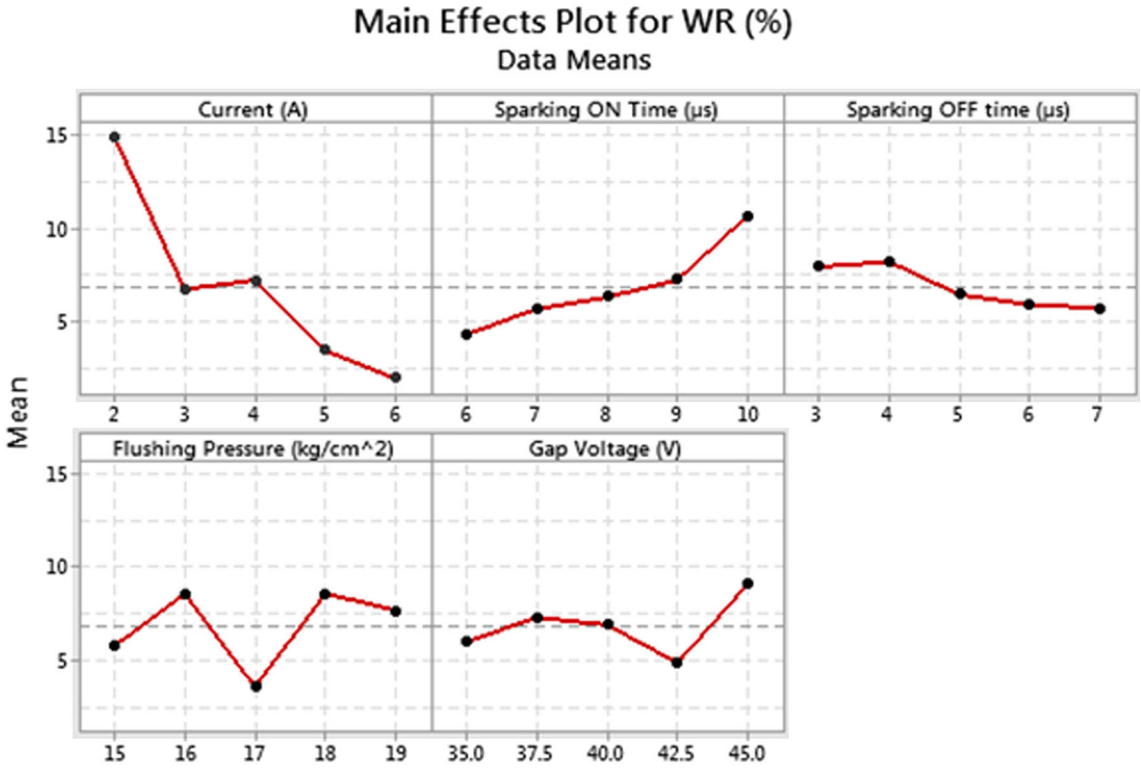

Fig. 17 Mean effect plot for runout

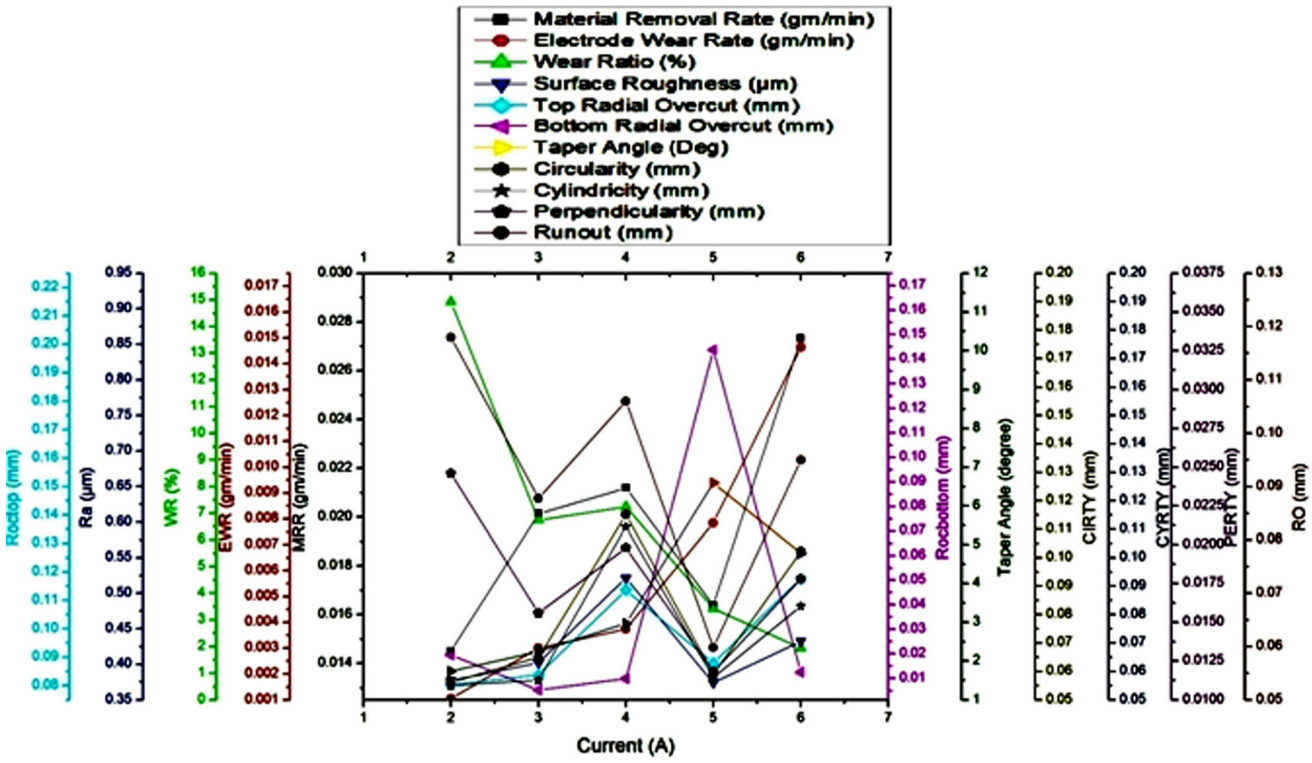

Fig. 18 Current (A) vs. measurements parameters

2.1.10 Wear Ratio. The main effects Fig. 16 shows that the least WR is achieved with the following parameters: current level 5 of 6A, pulse on time of 1 of 6 s, pulse off time of 5 of 7 s, dielectric pressure of 3 of 17 kg/cm^2, and spark gap voltage of 4 of 42.5 V.

2.1.11 Run Out. The major effects Fig. 17 show that the minimal runout occurs at a current of 4 at 5 A, a pulse on time of 1 at 6 s, a pulse off time of 1 at 3 s, a dielectric pressure of 5 at 19 kg/cm^2, and a spark gap voltage of 2 at 37.5 V.

2.2 Analysis of Input Parameter Versus Measuring Parameter on EDM of $MoSi_2$-SiC Ceramics Composites

Output process parameters shown in Fig. 18, 19, 20, 21, and 22 include material removal rate (g/min), electrode wear ratio (g/min), wear ratio (%), surface roughness (m), top radial overcut (mm), bottom radial overcut (mm), taper angle (degree), circularity (mm), cylindricity (mm), perpendicularity (mm), and run out (mm) for drilling a 5-mm-diameter hole at 75 mm depth.

- Increasing the current level results in a higher MRR because more energy is available to melt and evaporate the substance.
- A shorter pulse on time may reduce EWR because the dielectric fluid has less time to flush out the debris, resulting in less erosion of the electrode.
- With a shorter pulse off time during the electrical discharge, melting and vaporization of the material may be reduced, as can surface roughness.
- Material removal is consistent, and top radial overcut is kept to a minimum because of the uniform electric field produced by the high dielectric pressure level of 19 kg/cm^2.
- Bottom radial overcut is minimized and unnecessary material removal is prevented by setting the spark gap voltage to 37.5 V.
- The shortest taper angle was found for a certain range of values for the input process parameters.
- The electrode's shape and size affect the spark discharge and material removal rate, which in turn are determined by the precise combination of input process parameters that yields minimum circularity.
- Cylindricity: The current level of 1 A may be suitable for achieving minimum cylindricity, as it provides sufficient energy for the machining operation to remove material without generating excessive deformation or distortion of the workpiece.
- The current makes everything more perpendicular. The perpendicularity also increases when the Current level is raised from 2 to 3.

2.3 Steps to Successful Optimization Gray Relation Analysis (GRA)

Gray relational analysis (GRA) is one way to think about how unclear data is. GRA not only looks at how closely two sequences are related to each other, but it also looks at how much data is different between the two sequences. The GRA method includes finding the highest normalized value, regardless of response variables, trials, etc., finding the absolute difference between each normalized value and the highest value, and figuring out the gray relational coefficient for each normalized value. Lastly, the gray relational grade for each run of an experiment is found by adding the gray relational coefficients for each answer. Using gray relational assessment,

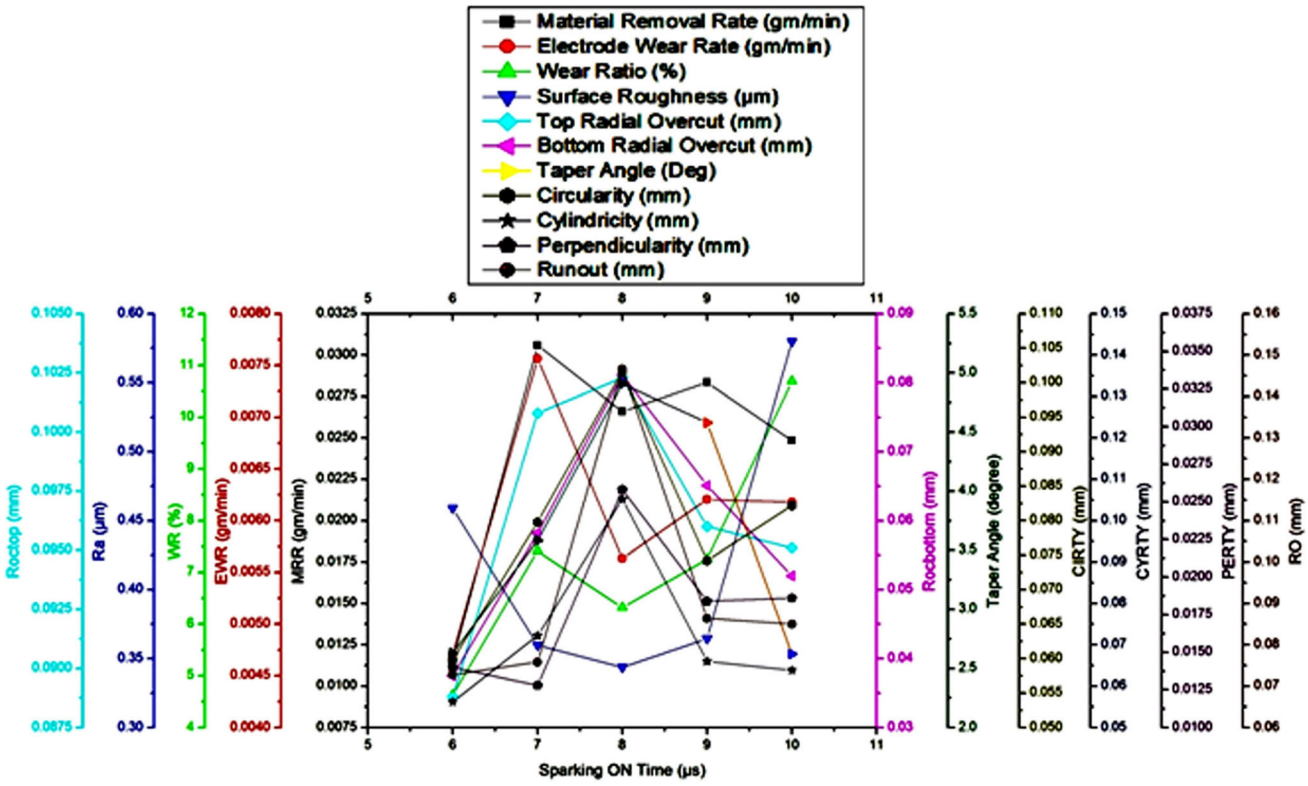

Fig. 19 Pulse on time (μs) vs. output parameters

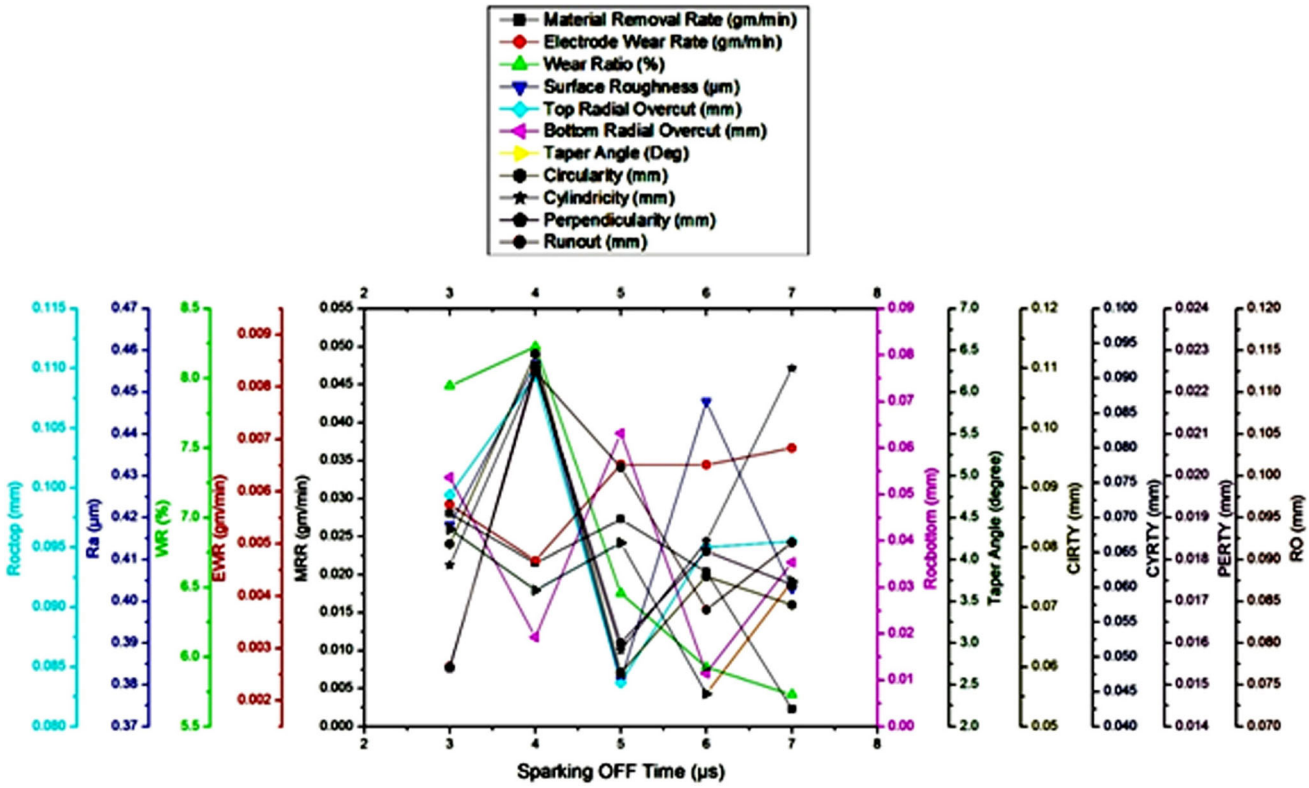

Fig. 20 Pulse off time (s) vs. output parameters

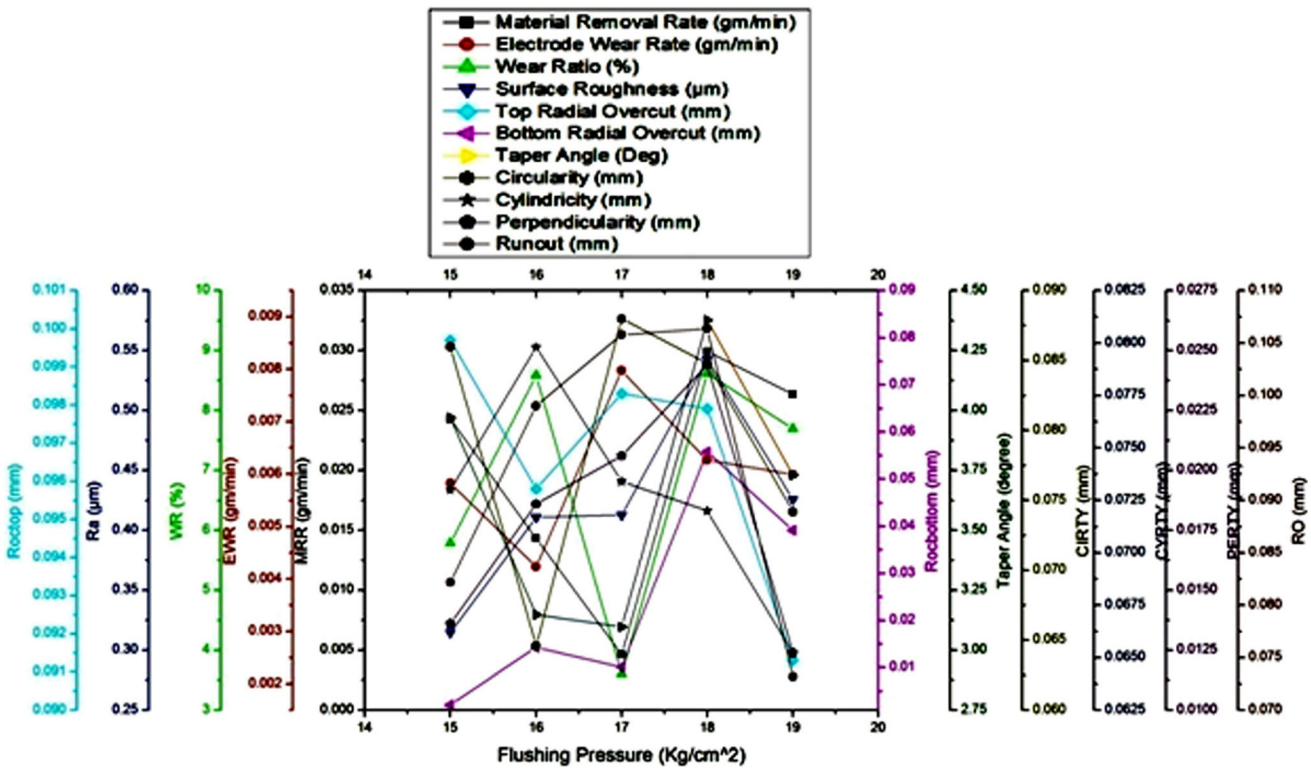

Fig. 21 Flushing pressure (kg/cm^2) vs. output parameters

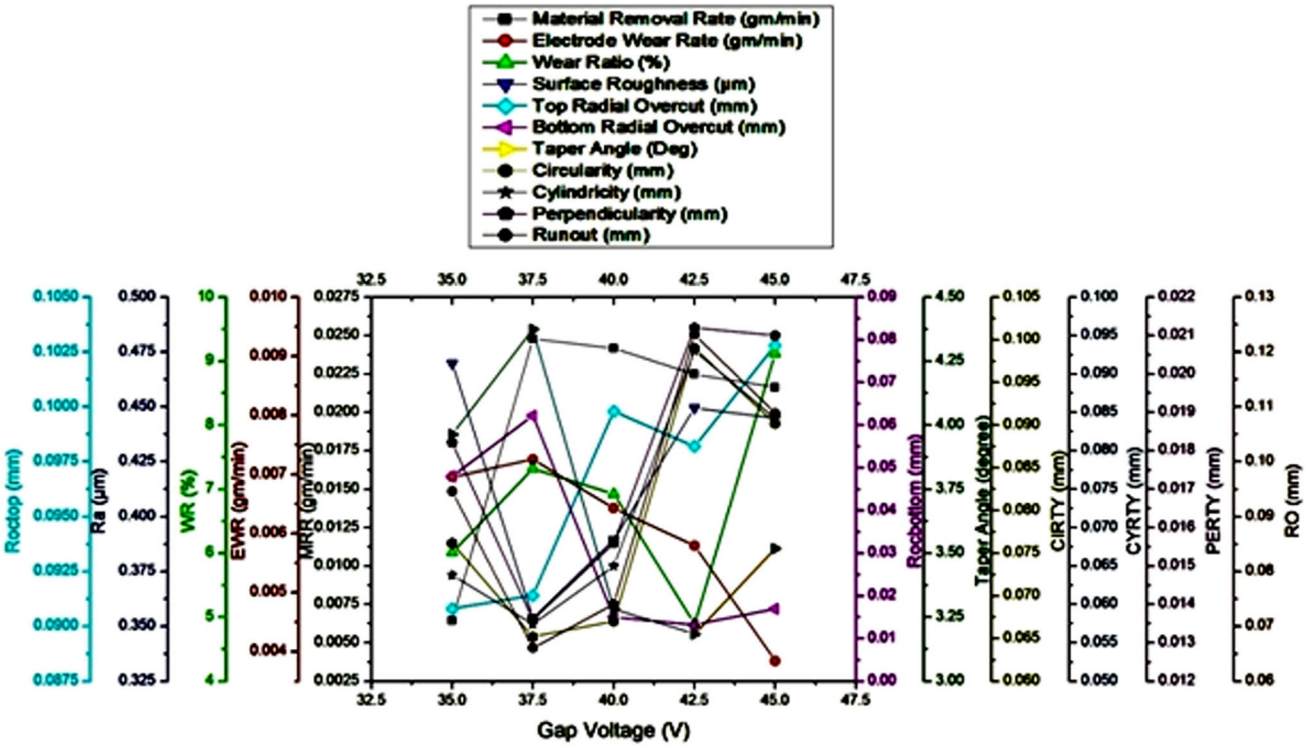

Fig. 22 Gap voltage (V) vs. output parameters

turn the multi-objective problem into a single optimization problem and use it to look at the experimental data. Standard methods for gray relational analysis were used to figure out the overall gray grade.

Step 1 Apply Eq 7 and 8 to get the signal-to-noise ratio for relating experimental results.

i. Higher—the—better

$$S/N \text{ ratio } (\eta) = -10\log_{10}\left(\frac{1}{n}\right)\sum_{i=1}^{n}\frac{1}{y_{ij}^2} \quad \text{(Eq 7)}$$

where *S*/*N* ratio is the resultant, n is the number of observations, and y is the response.

The MRR in this analysis is of the more, the better kind. This led us to use Eq 7 to determine the *S*/*N* ratios of the MRR and WR.

$$S/N \text{ ratio } (\eta) = -10\log_{10}\left(\frac{1}{n}\sum_{i=1}^{n}y_{ij}^2\right) \quad \text{(Eq 8)}$$

Productivity, dimensional deviation, and surface roughness are all instances of performance measurements where smaller is better. Therefore, the *S*/*N* values of experimental data may be evaluated using Eq 7 and 8.Table 3 shows the signal-to-noise ratio values for different trails.

Step 2: Experiment data is standardized for each possible response. Input data (y_{ij}) is transformed (using an equation) into output data (X_{ij}, $0X_{ij1}$), which may then be shared and evaluated in a larger study. Reducing the number of variables by picking numerous components is unnecessary. When analyzing information using gray theory or another method, normalization is a prerequisite. When subtracting the value of one array from another, an estimate of an array that is near 1 may be used. The conventional method's responsiveness to the course outcome was also studied since normalization alters grades. This means that the signal-to-noise ratio (*S*/*N*) must be taken into account while doing data normalization.

$$X_{ij} = \frac{y_{ij} - \min\left(y_{ij}, i = 1,2,\ldots n\right)}{\max\left(y_{ij}, i = 1,2,\ldots n\right) - \min\left(y_{ij}, i = 1,2,\ldots n\right)}$$

(Signal to noise ratio with Higher the greater mode) (Eq 9)

$$X_{ij} = \frac{\max\left(y_{ij}, i = 1,2,\ldots n\right) - y_{ij}}{\max\left(y_{ij}, i = 1,2,\ldots n\right) - \min\left(y_{ij}, i = 1,2,\ldots n\right)}$$

(Signal to noise ratio with lower the greater mode) (Eq 10)

Equation 9 was used to maximize the performance characteristics, and Eq 10 was used to reduce the performance characteristics to get the normalized values of the experimental data.

Step 3 Calculate the gray relational coefficient in normalization results.

$$\gamma(y_0(k), y_i(k)) = \frac{\Delta\min + \xi\Delta\max}{\Delta_{oj}(k) + \xi\Delta\max} \quad \text{(Eq 11)}$$

The defined range of $0 \leq \xi \leq 1$ determines differentiated of coefficient. The results are given in Table 4.

Step 4 Determination of gray grades:

$$\overline{\gamma_J} = \frac{1}{k}\sum_{i=1}^{m}\gamma_{ij} \quad \text{(Eq 12)}$$

Table 3 Signal-to-noise ratio values for different trails

S/N ratio											
S. No.	**MRR**	**EWR**	**WR**	**Ra**	**ROC_{TOP}**	**ROC_{BOT}**	**θ**	**CIRTY**	**CYRTY**	**PERTY**	**RO**
1	− 37.8910	58.7504	20.8594	11.8692	23.6752	34.6566	− 2.5822	30.7520	32.0412	36.4782	20.4455
2	− 42.0925	67.4827	25.3903	12.9950	19.3315	29.1186	− 6.4045	25.3521	25.1927	34.4249	21.6184
3	− 34.6549	56.6246	21.9697	9.6297	22.7335	42.4988	− 5.4636	23.3498	24.0132	29.1186	14.4708
4	− 33.2524	55.4352	22.1829	5.5473	21.8841	53.9794	− 7.0348	22.4988	22.7335	29.1186	17.3292
5	− 38.7181	64.5632	25.8451	5.2403	22.6154	29.2436	− 1.0727	25.1927	24.5830	34.4249	21.2096
6	− 52.9563	50.9540	− 2.0023	6.0729	21.1598	23.4139	4.8378	19.4939	23.0980	34.4249	19.0156
7	− 29.0819	47.8657	18.7837	9.1934	22.4411	36.1934	− 8.3167	26.1961	26.0206	34.4249	17.7211
8	− 32.2500	48.5662	16.3162	8.9954	20.5838	44.4370	− 9.0912	23.3498	24.8825	35.3910	20.1755
9	− 33.4684	50.5545	17.0861	11.5679	22.4988	26.1079	− 11.0340	24.8825	24.7314	39.1721	24.7314
10	− 35.0802	56.7539	21.6736	5.2403	21.2096	30.4576	− 4.2570	26.9357	26.1961	38.4164	27.7443
11	− 35.2781	47.8614	12.5832	6.2316	21.7237	25.4329	− 11.7674	24.5830	24.2934	47.9588	28.6360
12	− 33.8701	43.4125	9.5424	9.1186	18.5624	26.1961	− 5.9154	19.5762	21.2096	46.0206	29.8970
13	− 36.5479	50.2235	13.6756	9.2436	19.0156	33.9794	− 8.4115	18.3443	14.2440	29.8970	13.2708
14	− 30.9540	50.0389	19.0849	7.3711	17.0465	47.9588	− 12.3241	18.1316	20.2646	33.1515	20.3546
15	− 31.9545	55.5371	23.5826	0.0261	18.7484	28.4043	− 6.9235	15.5457	18.7860	28.8739	16.5948
16	− 45.0640	60.1566	15.0926	4.9898	22.0475	32.5786	− 9.3487	26.9357	24.7314	35.9176	23.3498
17	− 25.0437	37.7055	12.6619	8.7304	21.2597	16.0544	− 16.8468	24.5830	22.0475	40.9151	26.7448
18	− 26.4264	40.5228	14.0964	9.1435	21.1103	11.0879	− 20.3391	22.7335	25.1927	35.9176	23.6091
19	− 26.9845	41.9483	14.9638	12.8795	20.8192	17.2656	− 16.2631	24.8825	24.5830	40.0000	25.0362
20	− 28.0076	42.1680	14.1604	8.7541	20.4455	18.3085	− 15.8173	24.2934	28.4043	41.9382	24.0132
21	− 34.0937	36.7668	2.6731	6.1431	17.7211	32.2167	− 12.9032	24.4370	23.4785	35.9176	25.6799
22	− 29.4360	37.3358	7.8997	5.8146	18.7108	29.3704	− 12.6474	17.5885	20.9151	38.4164	21.1103
23	− 31.2207	39.6033	8.3826	9.3960	16.7726	20.6303	− 16.6326	14.9916	16.0820	30.7520	15.7562
24	− 31.8054	36.3464	4.5410	8.4962	20.6303	17.5230	− 16.1873	24.7314	27.3306	37.0774	21.3100
25	− 30.4725	34.2426	3.7700	7.0719	19.6593	28.8739	− 5.7887	21.6184	24.7314	34.8945	21.3100

Table 4 Computes the gray relational coefficient (GRC) for various paths

Gray relational coefficient											
S. No.	**MRR**	**EWR**	**WR**	**Ra**	**ROC_{TOP}**	**ROC_{BOT}**	**θ**	**CIRTY**	**CYRTY**	**PERTY**	**RO**
1	0.5207	0.4041	0.7363	0.3538	0.3333	0.4764	0.4148	0.3333	0.3333	0.5565	0.5368
2	0.4501	0.3333	0.9684	0.3333	0.5742	0.5433	0.4746	0.4320	0.4484	0.6322	0.4990
3	0.5922	0.4261	0.7823	0.4031	0.3667	0.4057	0.4584	0.4853	0.4767	0.9750	0.8739
4	0.6297	0.4395	0.7918	0.5401	0.4031	0.3333	0.4862	0.5121	0.5118	0.9750	0.6720
5	0.5051	0.3541	1.0000	0.5543	0.3713	0.5415	0.3952	0.4358	0.4626	0.6322	0.5115
6	0.3333	0.4986	0.3333	0.5175	0.4403	0.6350	0.3333	0.6364	0.5013	0.6322	0.5913
7	0.7756	0.5495	0.6635	0.4143	0.3784	0.4607	0.5115	0.4129	0.4304	0.6322	0.6513
8	0.6595	0.5371	0.5937	0.4196	0.4752	0.3914	0.5281	0.4853	0.4555	0.5942	0.5463
9	0.6236	0.5047	0.6138	0.3597	0.3761	0.5881	0.5750	0.4434	0.4590	0.4810	0.4204
10	0.5817	0.4247	0.7695	0.5543	0.4375	0.5254	0.4391	0.3975	0.4268	0.5000	0.3648
11	0.5769	0.5496	0.5122	0.5110	0.4108	0.5992	0.5949	0.4510	0.4696	0.3333	0.3511
12	0.6126	0.6444	0.4606	0.4163	0.6585	0.5867	0.4660	0.6322	0.5609	0.3575	0.3333
13	0.5482	0.5098	0.5336	0.4130	0.6061	0.4837	0.5135	0.7015	1.0000	0.9032	1.0000
14	0.7025	0.5127	0.6732	0.4689	0.9265	0.3677	0.6110	0.7151	0.5965	0.6905	0.5399
15	0.6688	0.4384	0.8602	1.0000	0.6359	0.5533	0.4841	0.9343	0.6621	1.0000	0.7144
16	0.4108	0.3907	0.5643	0.5664	0.3955	0.4995	0.5339	0.3975	0.4590	0.5753	0.4520
17	1.0000	0.8276	0.5137	0.4269	0.4348	0.8120	0.7828	0.4510	0.5328	0.4421	0.3816
18	0.9099	0.7258	0.5424	0.4156	0.4431	1.0000	1.0000	0.5044	0.4484	0.5753	0.4457
19	0.8779	0.6832	0.5613	0.3353	0.4603	0.7764	0.7554	0.4434	0.4626	0.4617	0.4140
20	0.8248	0.6771	0.5437	0.4263	0.4844	0.7481	0.7357	0.4586	0.3859	0.4221	0.4363
21	0.6066	0.8681	0.3753	0.5146	0.7844	0.5037	0.6287	0.4548	0.4907	0.5753	0.4012
22	0.7606	0.8431	0.4369	0.5284	0.6404	0.5398	0.6207	0.7521	0.5715	0.5000	0.5147
23	0.6932	0.7561	0.4436	0.4090	1.0000	0.6921	0.7725	1.0000	0.8288	0.8356	0.7698
24	0.6736	0.8876	0.3952	0.4336	0.4722	0.7692	0.7520	0.4472	0.4048	0.5377	0.5084
25	0.7199	1.0000	0.3868	0.4793	0.5445	0.5466	0.4639	0.5432	0.4590	0.6131	0.5084

where $\overline{\gamma_j}$-Gray relation rank for the jth test. k—Number of output parameters. From obtained value in gray rank in Table 5.

Step 5. Maximizing gray rank values led to the discovery of the ideal parameter settings ($A_3B_3C_5D_4E_2$), which are shown in Table 6 and Fig. 23.

Step 6: Determine the significant parameters using ANOVA.

This analysis is a version of a static process analysis, which produces results based on a set of predetermined parameters. The results of the ANOVA test show how much weight each parameter has on the outcomes. Due to limitations in the Taguchi method, it is not possible to monitor progress in each parameter as the process unfolds. Thus, a proportional ANOVA is employed to get a fair outcome. When the F value is large, a shift in the erosion parameters produces very different outcomes. The GRG ANOVA data is shown in Table 7. Figure 24 highlights the significance of current, sparking ON time, and flushing pressure on the GRG.

Step 7. The projected optimal condition is calculated.

An optimally chosen machining stage not only predicts but also checks a confirmation feature that makes use of an optimally chosen design stage. Therefore, the optimal stage of the machining settings is calculated by utilizing formula (13) and the anticipated S/N ratio.

$$\hat{\eta} = \eta_m + \sum_{i=1}^{q} (\overline{\eta} - \eta_m) \quad \text{(Eq 13)}$$

η_m = Average S/N ratio, $\overline{\eta}$ = means S/N ratio relating to ith important parameter on jth Stage. q = The number of significant parameters.

Table 5 Gray relational grade

Ex. No.	Gray grade	Rank
1	0.4545	25
2	0.5172	18
3	0.5678	11
4	0.5722	8
5	0.5240	16
6	0.4957	20
7	0.5346	15
8	0.5169	19
9	0.4950	21
10	0.4928	22
11	0.4872	23
12	0.5208	17
13	0.6557	3
14	0.6186	5
15	0.7229	2
16	0.4768	24
17	0.6005	7
18	0.6373	4
19	0.5665	12
20	0.5585	14
21	0.5640	13
22	0.6098	6
23	0.7455	1
24	0.5711	9
25	0.5695	10

3. Test for Verification

The gray relational rank was computed using formula (9) and the optimal set of machining parameters related to the different response characteristics. The validation experiment, conducted using spark EDM, verifies and enhances the performance properties of ceramic composites. The gray relational rank for multi-performance enhancements of the spark eroding process also increased, from 0.7455 to 0.7782. Therefore, spark EDM, which has been optimized in many response optimizations using GRA, is the exploratory result in machining parameters. The result of the validation trial is shown in Table 8.

3.1 Microstructural Analysis of Drilled Hole

The microstructural characterization of spark-machined composite material is shown in Fig. 25(a), (b), and (c). Those figures suggest that craters, globules, microholes, and fractures occur. Craters, globules, microvoids, and fractures occur differently on each machined surface, as seen in Fig. 25(a), (b), and (c). Craters are formed due to high thermal energy and peak current. An increase in dielectric fluid pressure resulted in an increase in the craters on the workpiece surface due to the high discharge energy. Globules are formed due to the presence of surface tension in the molten metal. Microvoids increase with an increase in pulse current and pulse on Time. If the composite material is not properly compacted or consolidated during the fabrication process, it can result in the formation of voids or microvoids. Craters, globules, and microvoids were reduced in size and quantity during stage 1 of the machining process, as shown in Fig. 25(a). As a consequence, short sparking lengths may lead to reduced vaporization on the workpiece's surface at machining stages I = 2 A, T_{on} = 6 s, T_{off} = 3 s, DP = 15 kg/cm^2, and V = 37.5 V, whereas longer sparking durations may lead to plasma channel expansion, decreasing the energy density in the machining process.

Table 6 Gray relational grade for response table

Factor	Gray relational grade					Optimum stages	Difference
	1	2	3	4	5		
'Current'	0.50886	0.56494	**0.63080**	0.57207	0.57754	3	0.12194
'Sparking ON time'	0.57229	0.53763	**0.62308**	0.53306	0.58816	3	0.09002
'Sparking OFF time'	0.57851	0.59242	0.55180	0.58885	**0.54263**	5	0.04979
'Flushing Pressure'	0.55982	0.55097	0.58064	**0.61355**	0.53923	4	0.07432
'Spark Gap Voltage'	0.56968	**0.61176**	0.55048	0.54823	0.57407	2	0.06353

Bold values indicate the level with the highest grey relational grade is the optimal level of the process parameters.

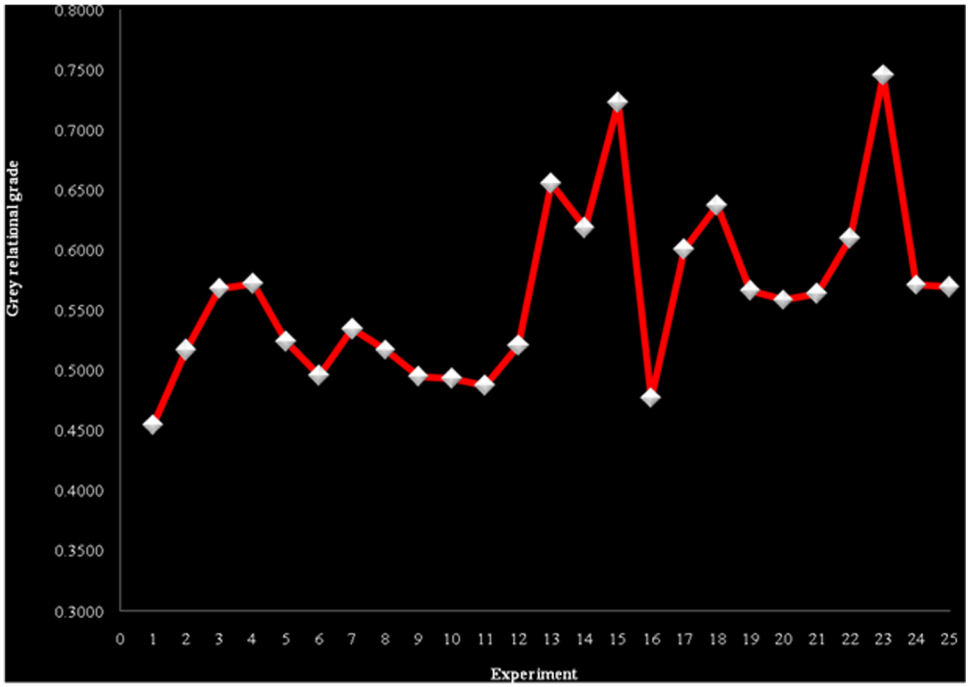

Fig. 23 Gray relation rank vs. experimental graph

Table 7 Gray relational grade for ANOVA results

Factor	SS	DOF	MS	*F* value	% contribution	Rank
'Current'	0.03759	4	0.00940	6.95939	34.6749	1
'Sparking ON time'	0.02781	4	0.00695	5.14811	25.6502	2
'Sparking OFF time'	0.01003	4	0.00251	1.85773	9.2561	5
'Flushing pressure'	0.01452	4	0.00363	2.68746	13.3902	3
'Spark gap voltage'	0.01306	4	0.00326	2.41772	12.0462	4
'Error'	0.00540	4	0.00135		4.9825	
'Total'	0.10841	24			100.0000	

SS sum of square, *DOF* degrees of freedom, *MS* mean square.
%-Percentage.

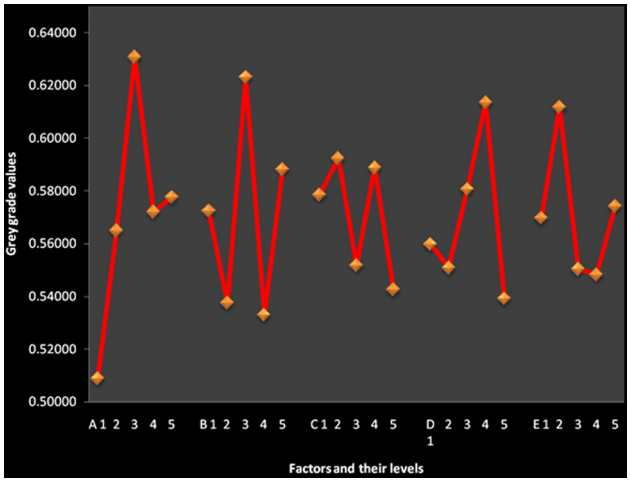

Fig. 24 Gray relation rank response graph

Machining Stage $I = 2$ A, $T_{on} = 6$ s, $T_{off} = 3$ s, DP = 15 kg/cm^2, and $V = 37.5$ V has a low electrical discharge energy, resulting in less material removal and less crater, microvoid, and globule development. For the parameters $I = 3$ A, $T_{on} = 7$ s, $T_{off} = 4$ s, DP = 16 kg/cm^2, and $V = 37.5$ V, a machined hole in a $MoSi_2$-SiC composite is shown in Fig. 25(b). A closer look at Fig. 25(b) reveals what seems to be an increase in the pace at which globules, microvoids, and craters are forming. Increases in current, sparking ON time, and voltage value have had an adverse effect on the machined surface.

Machining the composite material using di-sinking EDM at Stage $I = 4$ A, $T_{on} = 8$ s, $T_{off} = 5$ s, DP = 17 kg/cm^2, and $V = 40$ V yields the surface shown in Fig. 25(c). Stage $I = 2$ A, $T_{on} = 6$ s, $T_{off} = 3$ s, DP = 15 kg/cm^2, and $V = 35$ V seem to provide a surface that is somewhat rougher than the machined surface, as seen in the picture. This is because the minuscule holes and craters expanded in size as the sparking current increased. The MRR of the machined hole was found to be higher when a high sparking current was used because it generated greater plasma energy. In Fig. 25(c), we can see that

Table 8 shows the results of the validation trial

S. No	Response parameter	Machined parameters in 23rd trial	Optimal machining parameter	
			Prediction	Experiment
1	'Setting stage'	$A_5B_3C_2D_1E_5$	$A_3B_3C_5D_4E_2$	$A_3B_3C_5D_4E_2$
2	'Machining time (min)'	10.700	…	10.350
3	'Material removal rate (MRR) (gm/min)'	0.02748	…	0.03124
4	'Tool wear rate (TWR) (gm/min)'	0.01047	…	0.00181
5	'Wear ratio (WR)'	2.6250		3.5812
6	'Surface roughness (Ra)'	0.339		0.295
7	'Top radial overcut (ROC_{TOP}) (mm)'	0.1450		0.1395
8	'Bottom radial overcut (ROC_{BOT}) (mm)'	0.0930		0.0898
9	'Taper angle (θ)'	6.7863		5.8952
10	'Circularity (CIRTY) (mm)'	0.178	…	0.172
11	'Cylindricity (CYLTY) (mm)'	0.157	…	0.142
12	'Perpendicularity (PERTY) (mm)'	0.029	…	0.019
13	'Run out (RO)'	0.163		0.145
14	'Gray relational grade values'	0.7455	…	0.7782
Improvement in gray grades 0.0327.				

when the sparking ON time increases, the discharge energy at the spark gap increases as well, leading to the formation of microholes. Furthermore, as shown in Fig. 25(c), the crater enlargement is noticeably bigger than in Fig. 25(b). The reason for this is that the period of discharge energy increases along with the duration of the sparking ON time, allowing for more surface material removal and the creation of a hollow in the machined surface. Poor surface quality is produced when the residual unflushed material resolidifies on the machined surface in the form of a recast layer. Additionally, by creating more heat with a greater current, the heat has been conducted to a deeper layer, increasing the temperature.

Stage 4 machining of $MoSi_2$-SiC composite is seen in Fig. 25(d). Due to the increased current, sparking ON time, and voltage value, the machined surface now exhibits a higher density of craters, microvoids, and globulus compared to the machined surface seen in Fig. 25(c). This is because the discharge energy causes the machined surface to become uneven with increases in current, sparking ON time, and voltage.

At $I = 6$ A, $T_{on} = 10$ s, $T_{off} = 7$ s, DP = 19 kg/cm^2, and $V = 45$ V, the machined surface is shown in Fig. 25(e). Microholes and craters are most numerous in Fig. 25(e), as compared to the other figures in the same set (a-d). At $I = 6$ A, the crater's size has increased. Because of the high quantity of heat energy produced by the increased current, the surface quality suffered. For $I = 6$ A, the average size of the microvoids is larger than it is at $I = 2$ A, 3 A, 4 A, or 5 A. This is because, in comparison with $I = 2$ A, 3 A, 4 A, and 5 A, the greater sparking current formed more plasma channels on the surface of the work piece, resulting in the loss of a significant quantity of material and the growth of the crack density. An increasing quantity of thermoelectric energy was produced at the spark gap as the peak current increased. The material's surface quality is also affected. In addition, microfracture density increased with increase in sparking ON time. At high sparking ON time, strain on the machined surface exceeds the ultimate stress of the composite materials, leading to tiny fractures.

When the sparking ON time was prolonged, the crater and microvoid sizes grew. Specifically, longer discharge energies were maintained during longer sparking ON times. High gap voltage also results in a poorly machined surface. The surface quality was altered because of the high gap voltage, which caused a huge quantity of spark energy. At $I = 6$ A, $T_{on} = 10$ s, $T_{off} = 7$ s, DP = 19 kg/cm^2, and $V = 45$ V, a powerful blasting force was generated, which altered the machined surface. Taking these two factors into account, we have successfully achieved an uneven machined surface.

4. Conclusions

The following conclusions were reached after using gray techniques for multi-parametric optimization of $MoSi_2$-SiC ceramic composites with a copper electrode:

- Factor-level parameters control the ideal combination of outcomes. The optimal combination of results was created as $A_5B_3C_2D_1E_5$, which corresponds to the 23rd possible combination of parameters in an experiment.
- Specifically, the gray relational analysis discovered that the optimal values for the following parameters are as follows: current (I) = 4 A, sparking ON time (T_{on}) = 8 μs, sparking OFF time (T_{off}) = 7 μs, flushing pressure (DP) = 18 kg/cm^2, and spark gap voltage (V) = 37.5 V.
- This study assessed the significance of the following Spark EDM process characteristics using a gray relational grading system: peak current, sparking ON time, sparking OFF time, flushing pressure, and gap voltage. This method may be used to choose optimal EDM process settings from among several possible permutations.
- Sparking current (A = 35%), spark gap set voltage (D = 12%), flushing pressure (E = 13%), and sparking ON/OFF time (C = 9%) are the five most important variables in determining machining performance, in the order listed.

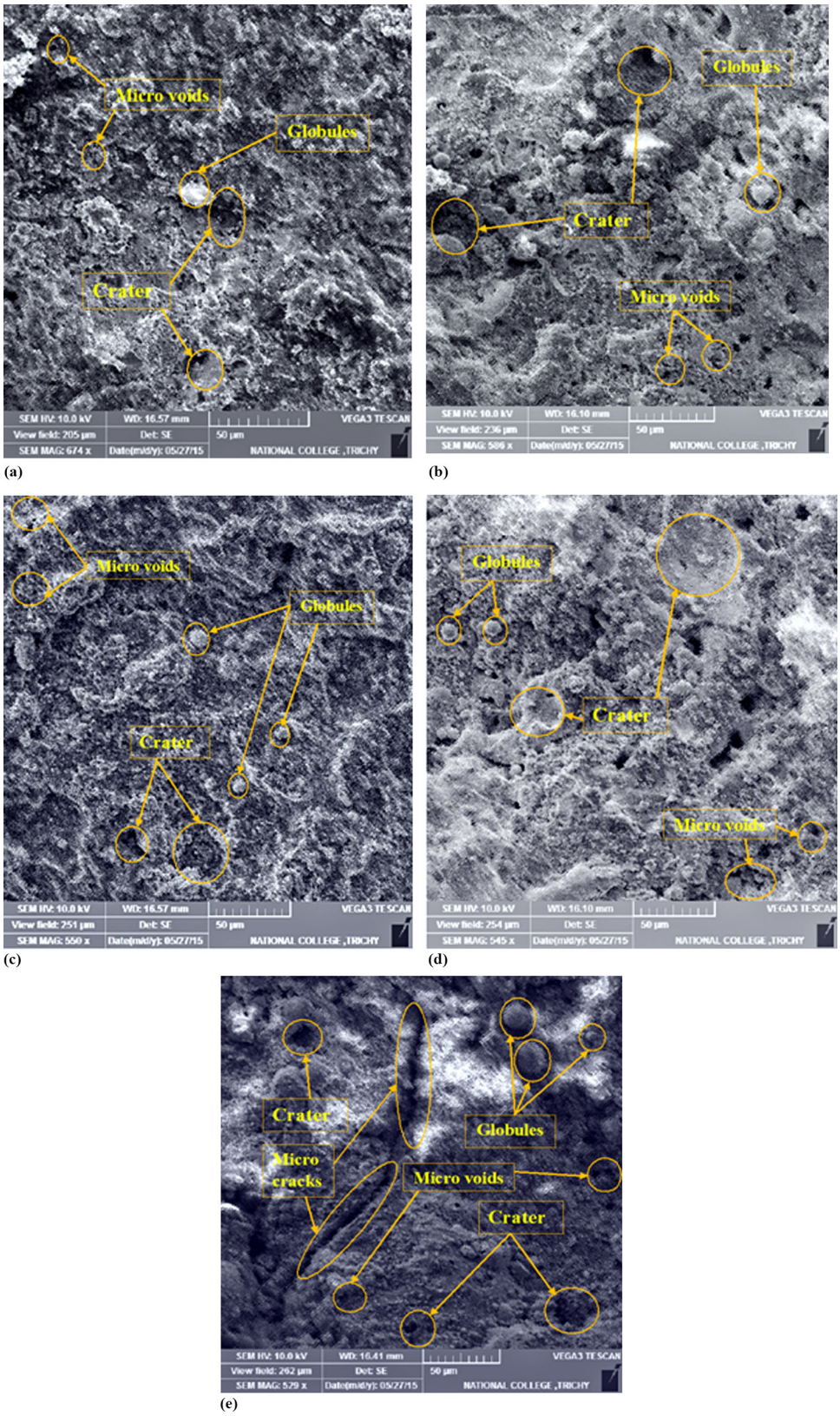

Fig. 25 Microstructural analysis of machined holes of $MoSi_2$-SiC composite by die-sinking EDM at (a) $I = 2$ A, $T_{on} = 6$ μs, $T_{off} = 3$ μs, DP = 15 kg/cm^2 and $V = 37.5$ V, (b) $I = 3$ A, $T_{on} = 7$ μs, $T_{off} = 4$ μs, DP = 16 kg/cm^2 and $V = 37.5$ V, (c) $I = 4$ A, $T_{on} = 8$ μs, $T_{off} = 5$ μs, DP = 17 kg/cm^2 and $V = 40$ V, (d) $I = 5$ A, $T_{on} = 9$ μs, $T_{off} = 6$ μs, DP = 18 kg/cm^2 and $V = 42.5$ V and (e) $I = 6$ A, $T_{on} = 10$ μs, $T_{off} = 7$ μs, DP = 19 kg/cm^2 and $V = 45$ V

- Improvements in productivity, dimensional deviation, and surface roughness were seen in the experiments.
- The results of the experiments could have been predicted with 95% accuracy using the Gray Method. It was shown that the EDM procedure is quite precise, which corroborated the GRA findings.
- To maximize the effectiveness of the spark EDM process, numerous performance criteria have been merged into a single performance characteristic using the gray approach.
- Boosting output is a major advantage of the present investigation. At the same time, a certain degree of geometric accuracy is maintained. The developed technical environment in $MoSi_2$-SiC composite electrical discharge machining will serve as a vital and promising guideline in modern industrial applications for efficient precision job production.
- In conclusion, the GRA technique is the most practical and economical approach to determining optimal EDM parameters.
- This study's results might, therefore, aid manufacturers and other researchers in improving the geometrical accuracy and precision of machined through holes in MoSi2-SiC Intermetallic/ceramic composites.
- With longer sparking ON times, more material is removed from the work piece's surface, and a hollow is formed in the machined surface.
- Microcracks emerge on the machined surface because the sparking ON time was too long, exceeding the ultimate stress of the composite materials.
- In Stage 5, the fracture density is at its highest and material loss is at its greatest when the sparking current is at its highest.
- Large amounts of spark energy are generated at high gap voltage, leading to subpar surface quality.

References

1. L. Selvarajan, C. Sathiya Narayanan, and R. JeyaPaul, Optimization of EDM Parameters on Machining Si_3N_4-TiN Composite for Improving Circularity, Cylindricity, and Perpendicularity, *Mater. Manuf. Process.*, 2016, **31**(4), p 405–412. https://doi.org/10.1080/10426914.2015.1058947
2. P. Malhotra, N.K. Singh, R.K. Tyagi, and B.S. Sikarwar, Comparative Study of Rotary-EDM, Gas Assisted-EDM, and Gas Assisted Powder Mixed-EDM of the Hybrid Metal Matrix Composite, *Adv. Mater. Process. Technol.*, 2021, **7**(1), p 27–41.
3. S. Singh, B. Patel, R.K. Upadhyay, and N.K. Singh, Improvement of Process Performance of Powder Mixed Electrical Discharge Machining by Optimization: A Review, *Adv. Mater. Process. Technol.*, 2021, **8**(3), p 3074–3104.
4. V. Srinivasan, P. Mouri, P.K. Palani, and S. Balamurugan, Experimental Investigation on EDM of Si_3N_4-TiN Using Grey Relational Analysis Coupled with Teaching-Learning-Based Optimization Algorithm, *Ceram. Int.*, 2021, **47**(13), p 19153–19168.
5. V.P. Srinivasan and P.K. Palani, Surface Integrity, Fatigue Performance and Dry Sliding Wear Behaviour of Si_3N_4-TiN After Wire-Electro Discharge Machining, *Ceram. Int.*, 2020, **46**(8), p 10734–10739.
6. L. Selvarajan, P. Mouri, and R.R. Raja, Experimental Investigation of EDM Parameters on Machining Si_3N_4-TiN Conductive Ceramic Composite Using Hallow Tube Electrode for Improving Geometrical Accuracy, *Mater. Today Proc.*, 2018, **5**(2), p 8080–8088.
7. R. Rajavel, L. Selvarajan, G. Rajkumar, R. Raja, and A. Rakshna, Investigation on Machinability of Al 2024& 7.5% Si_3N_4 Metal Matrix Composite with PMEDM Using Taguchi Based GRA, *Mater. Today Proc.*, 2021, **46**, p 9449–9453.
8. V. Marrocco, F. Modica, V. Bellantone, V. Medri, and I. Fassi, Sparking-Type Influence on the Micro-EDM Milling Machinability of Si_3N_4-TiN Workpieces, *Micromachines*, 2020, **11**(10), p 932.
9. L. Selvarajan, R. Rajavel, B. Prakash, D.G. Mohan, and S. Gopi, Investigation on Spark Electrical Discharge Machining of Si_3N_4 Based Advanced Conductive Ceramic Composites, *Mater. Today Proc.*, 2020, **27**, p 2174–2178.
10. W. Ming, H. Jia, H. Zhang, Z. Zhang, K. Liu, J. Du, F. Shen, and G. Zhang, A Comprehensive Review of Electric Discharge Machining of Advanced Ceramics, *Ceram. Int.*, 2020, **46**(14), p 21813–21838.
11. Y. Jiang, D. Feng, H. Ru, W. Wang, and C. Zhang, Oxidation Protective ZrB_2-$MoSi_2$-SiC-Si Coating for Graphite Materials Prepared by Slurry Dipping and Vapor Silicon Infiltration, *Surf. Coat. Technol.*, 2018, **339**, p 91–100.
12. Y. Zhang, L. Yu, T. Fu, J. Wang, F. Shen, and K. Cui, Microstructure Evolution and Growth Mechanism of Si-$MoSi_2$ Composite Coatings on TZM (Mo-0.5 Ti-0.1 Zr-0.02 C) Alloy, *J. Alloys Compd.*, 2022, **894**, p 162403.
13. L. Selvarajan, C.S. Narayanan, and R. Jeyapaul, Optimization of Process Parameters to Improve form and Orientation Tolerances in EDM of $MoSi_2$-SiC Composites, *Mater. Manuf. Process.*, 2015, **30**(8), p 954–960.
14. L. Selvarajan, C. Sathiya Narayanan, and R. Jeyapaul, Optimization of EDM Hole Drilling Parameters in Machining of $MoSi_2$-SiC Intermetallic/Composites for Improving Geometrical Tolerances, *J. Adv. Manuf. Syst.*, 2015, **14**(04), p 259–272.
15. L. Selvarajan, C.S. Narayanan, R. Jeyapaul, and M. Manohar, Optimization of EDM Process Parameters in Machining Si_3N_4-TiN Conductive Ceramic Composites to Improve form and Orientation Tolerances, *Measurement*, 2016, **92**, p 114–129.
16. A.A.A. Alduroobi, A.M. Ubaid, M.A. Tawfiq, and R.R. Elias, Wire EDM Process Optimization for Machining AISI 1045 Steel by Use of Taguchi Method, Artificial Neural Network and Analysis of Variances, *Int. J. Syst. Assur. Eng. Manag.*, 2020, **11**(6), p 1314–1338.
17. R. Chaudhari, J. Vora, D.M. Parikh, V. Wankhede, and S. Khanna, Multi-Response Optimization of WEDM Parameters Using an Integrated Approach of RSM–GRA Analysis for Pure Titanium, *J. Inst. Eng. (India) Ser. D*, 2020, **101**(1), p 117–126.
18. J. Singh, G. Singh, and P.M. Pandey, Electric Discharge Machining Using Rapid Manufactured Complex Shape Copper Electrode with Cryogenic Cooling Channel, *Proc. IMechE Part B J. Eng. Manuf.*, 2021, **235**(1–2), p 173–185.
19. O. Belgassim and A. Abusaada, Investigation of the Influence of EDM Parameters on the Overcut for AISI D3 Tool Steel, *Proc. IMechE Part B J. Eng. Manuf.*, 2012, **226**(2), p 365–370.
20. L. Selvarajan, M. Manohar, and P. Dhinakaran, Modelling and Experimental Investigation of Process Parameters in EDM of Si_3N_4-TiN Composites Using GRA-RSM, *J. Mech. Sci. Technol.*, 2017, **31**(1), p 111–122.
21. L. Selvarajan, C. Sathiya Narayanan, and R. Jeyapaul, Multi-Objective Optimization on Electric Discharge Machining Using by Grey Relational analysis, *Appl. Mech. Mater.*, 2014, **592**, p 550–554.
22. L. Selvarajan, R. Rajavel, K. Venkataramanan, and V.P. Srinivasan, Experimental Investigation on Surface Morphology and Recasting Layer of Si_3N_4-TiN Composites Machined by Die-Sinking and Rotary EDM, *Ceram. Int.*, 2023, **49**(5), p 8487–8501. https://doi.org/10.1016/j.ceramint.2022.11.011
23. L. Selvarajan, K. Venkataramanan, R. Rajavel, and T.S. Senthilkumar, Fuzzy Logic Optimization with Regression Analysis on EDM Machining Parameters of Si_3N_4-TiN Ceramic Composites, *J. Intell. Fuzzy Syst.*, 2023 https://doi.org/10.3233/JIFS-223650
24. L. Selvarajan and K. Venkataramanan, Si_3N_4-TiN Conductive Ceramic Composites: Topography on EDMed Surfaces and Precise Drilled Holes, *Mater. Sci. Technol.*, 2023 https://doi.org/10.1080/02670836.2023.2187156
25. L. Selvarajan, K. Venkataramanan, and T.S. Senthilkumar, Experimental Investigation and Optimization of EDM Performance Measures of $MoSi_2$-SiC Intermetallic Ceramic Composite Using RSM with Regression Equations, *SILICON*, 2023, **15**, p 1747–1769. https://doi.org/10.1007/s12633-022-02093-9

26. S.S. Sidhu and P.S. Bains, Study of the Recast Layer of Particulate Reinforced Metal Matrix Composites Machined by EDM, *Mater. Today Proc.*, 2017, **4**(2), p 3243–3251.
27. L. Selvarajan, C.S. Narayanan, and R. Jeyapaul, Optimization of EDM Parameters on Machining Si3N4-TiN Composite for Improving Circularity, Cylindricity, and Perpendicularity, *Mater. Manuf. Process.*, 2016, **31**(4), p 405–412.
28. A.K. Khanra, B.R. Sarkar, B. Bhattacharya, L.C. Pathak, and M.M. Godkhindi, Performance of ZrB_2-Cu Composite as an EDM Electrode, *J. Mater. Process. Technol.*, 2007, **183**(1), p 122–126.